CHARACTERIZING THE ACOUSTIC BEHAVIOR OF HEXAGONAL PERIODIC CELLULAR CORES

by

Ammar Ahmed

A Thesis Presented to the Faculty of Engineering
American University of Sharjah
College of Engineering
in Partial Fulfillment
of the Requirements
for the Degree of

Master of Science in
Mechanical Engineering

Sharjah, United Arab Emirates

December 2020

Declaration of Authorship

I declare that this thesis is my own work and, to the best of my knowledge and belief, it does not contain material published or written by a third party, except where permission has been obtained and/or appropriately cited through full and accurate referencing.

Signed Ammar Ahmed

Date: Nov. 27. 2020

Approval Signatures

We, the undersigned, approve the Master's Thesis of Ammar Ahmed

Thesis Title: Characterizing the Acoustic Behavior of Hexagonal Periodic Cellular Cores

Date of Defense: Thursday, Dec. 10. 2020

Name, Title and Affiliation	**Signature**
Dr. Maen Alkhader Associate Professor, Department of Mechanical Engineering Thesis Advisor	
Dr. Bassam Abu-Nabah Associate Professor, Department of Mechanical Engineering Thesis Co-Advisor	
Dr. Wael Abuzaid Assistant Professor, Department of Mechanical Engineering Thesis Committee Member	
Dr. Farid Abed Professor, Department of Civil Engineering Thesis Committee Member	
Dr. Mamoun Abdel-Hafez Head Department of Mechanical Engineering	
Dr. Lotfi Romdhane Associate Dean for Graduate Affairs and Research College of Engineering	
Dr. Sirin Tekinay Dean College of Engineering	
Dr. Mohamed El-Tarhuni Vice Provost for Graduate Studies Office of Graduate Studies	

Acknowledgement

First and foremost, I would like to express my sincere thanks to my advisors Dr. Maen Alkhader and Dr. Bassam Abu-Nabah for their time, efforts, continuous support and help throughout the thesis. I would like also to thank my thesis committee members Dr. Wael Abuzaid and Dr. Farid Abed for their support and constructive instructions. I would like to express my sincere appreciations to AUS for granting me a Graduate Teaching Assistantship during my study. I am indeed thankful to all faculty and staff members in the Mechanical Engineering Department at AUS for their support and considerate guidance. Further, I would like to thank all my family members and friends for their great support.

Abstract

Cellular solid cores are used in composite sandwich structures due to their high stiffness to weight ratio. However, owing to their porosity, they are inherently weak and are susceptible to damage due to improper loadings. As damaged cores can potentially lead to the failure of sandwich structures, core damage should be detected, preferably using nondestructive evaluation techniques. However, common nondestructive techniques, such as ultrasound, have limited effectiveness in inspecting cellular cores due to their dispersive properties. Since cellular cores are less dispersive at sub-ultrasound frequencies, inspecting them using sub-ultrasound frequencies has been introduced as a promising alternative to ultrasound inspection. However, this approach requires a priori knowledge of the acoustic characteristics in the inspected material, which is not available for most available cores. This work utilizes finite element computations to characterize the low frequency acoustic characteristics, namely phase velocity and dispersive properties, in commercial aluminum honeycombs made by bonding thin corrugated sheets. Results illustrate that the dispersive behavior and acoustic anisotropy of the studied honeycombs are more significant at higher porosities and higher frequencies. Moreover, results identify the frequencies below which honeycombs are least dispersive. To allow for realizing cores with tunable acoustic properties, the effect of admissible deformation modes, density, and geometric features on the phase velocities and dispersive properties is investigated. Accordingly, the acoustic behavior of honeycomb-based lattices that promote the two main admissible deformation modes in cellular solids, namely bending and stretching modes, is investigated. Results show that asymmetric waves in the bending dominated lattice are more direction dependent and less dispersive than in the stretching dominated lattice, whereas symmetric waves are generally independent of direction and dispersive in bending and stretching lattices. Results show that phase velocities of symmetric and asymmetric waves scale linearly with relative density in the bending dominated lattice and nonlinearly with relative density in the stretching dominated lattice; however, maximum phase velocities are higher in the stretching dominated lattice.

Keywords: ***Aluminum honeycombs; wave propagation; dispersion; non-destructive testing***

Table of Contents

List of Figures

List of Tables

Chapter 1. Introduction

In this chapter an introduction about the importance of sandwich structures and cellular cores to industries prioritizing weight minimization is presented. Then, the importance of understanding and characterizing the acoustic properties of cellular cores is highlighted. Subsequently, the addressed problem and the research contributions of this work are presented. Finally, the organization of this thesis is presented.

1.1. Overview

Due to their ability to provide excellent stiffness and strength to weight ratios, fiber composite materials are increasingly being used to replace steel and metallic alloys in aerospace, automotive and marine applications [1, 2]. In these applications, fiber composites are often used in a sandwich structure configuration. This particular configuration allows for capitalizing on fiber composites' excellent structural properties. In a sandwich structure, a light weight core is sandwiched between two thin composite sheets. The sheets would provide the structural stiffness of the structure, while the core is used mainly to increase the composite sheets second moment of inertia and hold the sheets in their proper position. To minimize the weight of the composite sandwich structure, the core is required to have minimal weight. Accordingly, foams, cellular solids and honeycombs have been the most widely used materials in the role of cores of sandwich structures [3].

Although cores are not meant to carry significant forces in properly designed sandwich structures, due to inadvertent loadings or impacts they might be subjected to unintended loadings. These loads, even when small, might damage composite cores as they are inherently weak due to their porous nature. Detecting damage in cores is usually difficult as they are not readily observable to the naked eye, due to being tightly sandwiched between composite sheets. One promising method to detect damage in cores is through the use of elastic waves based non-destructive evaluation techniques [4]. These are similar to ultrasound techniques but operate at lower frequencies. Using these techniques is instrumentally dependent on knowing the acoustic properties of the medium being investigated for damage. However, the acoustic properties of most cores used in sandwich structures are not well-characterized, and their porous structures renders the behaviour of their acoustic properties complex and non-intuitive. This constitutes a major hurdle in utilizing elastic-based non-destructive evaluation methods

in characterizing damage sustained by cores of sandwich structures. This work aims to ameliorate this issue by providing a better understanding of the acoustic behaviour of porous cores; particularly, honeycomb-like materials.

1.2. Thesis Objectives

The motivation behind this research is that the acoustic properties of cores used in sandwich structures are not well understood or characterized. Moreover, models capable of predicting the dispersive and anisotropic behaviour of cores' phase velocities in terms of their densities and geometric properties are currently lacking. The main objective of this thesis is to characterize the dispersive and anisotropic behaviour of phase velocities in the most commonly used cores in sandwich structures in terms of their density and geometric features. A second objective of this work is to shed light on the effect of admissible deformation modes in cellular solids, namely stretching and bending, on their acoustic properties. Objectives of this work are accomplished using numerical computations that integrate Bloch wave theory [5, 6] with finite element simulations.

1.3. Research Contribution

The contributions of this research work are:

- Characterize the dispersive and anisotropic behaviour of low frequency elastic waves propagating in honeycomb-like materials, which are the most commonly used cores in sandwich structures.
- Quantify the effect of density and geometric features on the phase velocities of low frequency waves propagating in honeycomb-like materials.
- Characterize the behaviour of both longitudinal and shear waves in honeycomb-like cores at low frequencies.
- Shed light on the effect of admissible and dominant deformation modes in cellular solids on their acoustic properties.
- Create an enabling platform for realizing cellular cores with tunable acoustic properties. This is achieved by highlighting the effect of admissible defamation mechanisms, density, and geometric features on cellular solids acoustic properties.

1.4. Thesis Organization

This thesis is organized as: Chapter 2 provides detailed background and literature review about wave propagation in cellular cores. Chapter 3 describes the numerical methodology used in this work. Chapter 4 presents the results. Finally, Chapters 5 and 6 present the discussion and conclusions, respectively.

Chapter 2. Background and Literature Review

Composite sandwich structures are widely used as load bearing members in applications where flexural loading modes are dominant and weight reduction is required, such as in aerospace and wind energy applications [1, 2]. Sandwich structures are typically constructed by adhering two thin composite sheets to a thick, porous, light weight, and low strength core material that fill the space between the two composite sheets [2]. One of the most widely used core materials in sandwich structures is the class of materials referred to as aluminum honeycombs, which are very effective as cores due to their porous structure, very low density and better capacity to carry compressive and transverse loads than most polymeric core materials (e.g., rigid polymeric foams) [3, 7].

In a properly designed aluminum honeycomb based sandwich structure, the composite sheets provide the main load bearing capacity of the structure [1, 2], while the low weight honeycomb core is mainly responsible for increasing the sandwich structure's flexural rigidity (i.e., by increasing the second moment of inertia) and providing secondary supportive roles that do not require significant load carrying capacity. These supportive roles are critical to the functionality and integrity of composite sandwich structures, and they include: backing the composite sheets and preventing them from wrinkling, buckling, or bulging; supporting the composite sheets against non-flexural loads (e.g., compressive loads due to impact or concentrated forces); and ensuring that the two composite sheets deform simultaneously in a compatible manner. The aforementioned roles, though supportive, are critical. Unsatisfying them (e.g., due to a damaged core) will compromise the functionality and structural integrity of sandwich structures.

Owing to their porous structure, aluminum honeycombs, as all core materials, are inherently week and have high propensity to sustain damage or permanently deform under relatively small loads [8-13]. Thus, inadvertent and improper loadings (e.g., subjecting sandwich structures to minor impact) can potentially damage aluminum honeycomb cores in sandwich structures without damaging the composite sheets. However, loading a composite sandwich structure with a damaged core can lead to the failure of the composite sheets, and subsequently the failure of the whole sandwich structure. Thus, detecting, assessing, and if possible repairing any damage sustained by

cores in sandwich structures is critical to the integrity and durability of composite sandwich structures and applications utilizing them as load carrying members.

Cores in sandwich structures are inaccessible to the naked eye and inspecting them for damage requires nondestructive inspection and evaluation. However, most existing nondestructive evaluation (NDE) techniques have limited effectiveness in directly inspecting aluminum honeycombs, since their porous structure renders them very dispersive to ultrasound waves and distortive to electromagnetic fields [4]. Currently, damage in honeycomb cores is often indirectly inferred from changes in the mechanical or thermal behaviors of sandwich structures (e.g., through Shearography or Thermography). Nevertheless, the aforementioned indirect methods for damage detection mainly measure delamination at the core-composite sheet interfaces and are not compatible with continuous structural health monitoring. However, as aluminum honeycombs exhibit much less dispersive behavior at low and sub-ultrasound frequencies (5~50KHz) [4, 14], low frequency based inspection approach delivers a promising solution for direct inspection and continuous health monitoring applications [4]. This approach draws on the principles of Ultrasonic NDE methods but utilizes low sub-ultrasound frequencies, at which aluminum honeycombs exhibit relatively isotropic acoustic behavior and minimal transmission losses [4, 14].

Low sub-ultrasound frequency inspection approach, just like ultrasound techniques, requires having a priori knowledge of the wave propagation characteristics in the inspected media. This knowledge is partially available for few honeycombs and honeycomb-like materials. Wave propagation characteristics in cellular solids and honeycomb-like materials were investigated for auxetic [15], Chiral [16], Zig-Zag [17], tetragonal and triangular [18] structures. These studies highlighted the sensitivity of natural modes, phase velocities, and dispersion properties to the periodic topology of cellular structures and their length scales. Similarly, for honeycombs, their band gaps, phase velocities, and dispersion characteristics were found to be very sensitive to their constituent material, length scale and minor changes in their topology [15, 19] as well as to macroscopic strain (>1%) and porosity level [14, 20]. Most importantly, honeycombs were observed to exhibit a very dispersive behavior at high frequencies and almost non-dispersive behavior at very low frequencies [14, 19]. This transition from dispersive to non-dispersive behavior is very dependent on the relative density or

porosity [14, 19]. For instance, the frequency level at which the dispersive behavior commences increases with decreased porosity (i.e., increased relative density) [14, 19].

The aforementioned efforts were very effective in highlighting the dispersive and acoustic properties of honeycombs and cellular materials in general. However, they used idealized geometries that do not mirror the topological details (i.e., cell size, cell wall thickness) and porosity levels of commercially available aluminum honeycombs, which are mostly made by bonding corrugated thin sheets [3]. Most studies assumed cell walls to have uniform thickness (i.e., did not account for the doubled thickness at the cell walls resulting from the welding of the corrugated sheets), and they emphasized on high porosity levels, which are not representative of commercially available aluminum honeycombs. Thus, it can be concluded that the low frequency wave propagation characteristics in commercially available aluminum honeycombs remain not fully characterized, particularly for the ones widely used in sandwich structures and made by bonding thin corrugated sheets. The lack of this knowledge hinders the use of low frequency (i.e., <1 MHz) elastic waves based nondestructive methods in inspecting aluminum honeycomb cores for defects.

Accordingly, this work aims to provide detailed characterization of the low frequency wave propagation characteristics (i.e., frequency-dependent wave dispersion and phase velocities) in commercially available aluminum honeycombs, particularly the ones made by Hexel Corporation as they constitute the standard aluminum honeycomb cores used in the aerospace industries worldwide. For this end, this work systematically analyzes, using finite element computations and Bloch wave theory [5, 6], the in-plane wave propagation in realistic aluminum honeycomb models that mirror the features of honeycombs made by bonding corrugated aluminum sheets. Resulting data should assist in the advancement of nondestructive inspection techniques tailored for aluminum honeycombs and porous media. For instance, results would assist in selecting the test frequencies, positioning sensors and wave sources as well as in data interpretation. Finally, advancing the field of nondestructive evaluation of honeycomb cores will assist in characterizing damage in cellular solids used in other applications, such as in active brittle piezoelectric ceramic cellular solids, which are increasingly being considered as emerging metamaterials for sensors [21-25].

The significant dependence of periodic cellular solids' acoustic properties on their lattice architecture and topology motivated exploring the sensitivity of their acoustic properties to small and large deformation-induced changes in their topology. Accordingly, the sensitivity of periodic cellular solids' acoustic properties to both damage induced [14] and buckling triggered [26] changes in their topology were investigated. Results revealed that small variation in periodic lattices' topology (in the order of about 2% macroscopic permanent strain) is associated with small but measurable changes in their phase velocities and frequency band gaps, while large variation in their topology (>30% macroscopic permanent strain) is associated with significant (order of magnitude) changes in their phase velocities and frequency band gaps [14, 26]. More importantly, the aforementioned results established that the acoustic properties of periodic cellular solids can be tuned through inducing deformations in their ligaments. This, in part, helped in motivating a thrust of efforts that aimed to develop piezoelectric based [27, 28] and shape memory based [24, 29, 30] cellular structures with tunable properties whose topology can transform through actively controlled deformations at their ligament level.

As acoustic properties of materials are inherently dependent on their stiffness, they are sensitive to parameters affecting it. For cellular solids, porosity is one of the most stiffness affecting parameters [3, 31, 32]; therefore, it could significantly affect cellular solids acoustic properties. Consequently, some efforts have been applied to characterize the effect of porosity on the acoustic properties of periodic cellular solids. These efforts utilized hexagonal topologies [14, 33] and demonstrated an increase in the dispersive behavior of cellular solids at higher porosities. Moreover, they showed that phase velocities of shear waves (asymmetric waves) scale inversely with porosity, while phase velocities of longitudinal waves (symmetric waves) are insensitive to porosity at small frequencies and inversely proportional to porosity at larger frequencies.

Similar to porosity, the underlying or admissible deformation modes in ligaments of periodic lattice architectures have a significant effect on lattices' stiffness [8, 9, 28, 34-36] and potentially on their acoustic behavior. Cellular solids, periodic and random, deform generally through the bending and stretching of their ligaments. However, only one of these modes dominates depending on cellular solids' topology

(i.e., nodal connectivity at vertices) and macroscopic deformation mode (e.g., shear or hydrostatic compression) [8, 9, 34]. Generally, lattices with high nodal connectivity (i.e. ≥ 6 lines per vertex in 2D) are always associated with a stretching dominated behavior, while lattices with low nodal connectivity (i.e., < 6 lines per vertex in 2D) are mostly associated with a bending dominated behavior [8]. The latter can still exhibit a stretching dominated behavior but only under certain macroscopic loading conditions (e.g., under hydrostatic loading [3]). The dominant deformation mode influences the behavior of cellular solids significantly [3]. For instance, stretching dominated cellular solids exhibit significantly higher specific stiffness and strength as compared to their bending dominated counterparts [8]. Moreover, stiffness of stretching dominated cellular solids scales linearly with porosity while it scales nonlinearly with porosity for their bending dominated counterparts [3, 8]. As acoustic properties of materials are dependent on parameters affecting their stiffness, the acoustic properties of periodic cellular solids such as dispersion, direction dependence, phase velocity, and band gaps are expected to be inherently dependent on the dominant deformation modes in their ligaments. This dependence was implicitly hinted to by Phani et al. (2006) [37] who investigated the behavior of band gabs in lattices with different nodal connectives. Their results showed that band gap characteristics are strongly sensitive to nodal connectivity (i.e., dominant mechanism), and they supported the hypothesis that one can, through tailor the periodic structure of cellular solids, design cellular solids with unique and application tailored acoustic properties. However, the relationship between periodic cellular solids' acoustic properties and their dominant deformation modes has not been fully investigated or characterized, particularly in terms of phase velocities and their behavior. Therefore, this work aims to provide insights into this relationship and to quantitatively measure the tunable range of honeycombs' acoustic behavior that can be realized through modifying their ligament structure and deformation mechanisms. Towards this end, this work computationally explores the effects of the dominant deformation modes (i.e., bending and stretching) in periodic honeycomb-like materials on the frequency and direction dependent behavior, particularly phase velocity, of in-plane waves traversing them. The approach used in this work is detailed next.

Chapter 3. Methodology

This work utilizes finite element computational models and Bloch wave theory to investigate the characteristics of low frequency elastic waves propagating in models mimicking aluminum honeycombs commonly used in composite sandwich structures. The computational approach is used, in particular, to simulate and characterize the wave propagation properties relevant to nondestructive testing applications, namely the phase velocities and dispersive characteristics of low frequency elastic waves as well as their dependence on propagation direction, topology, cell-size, and cell-wall thickness. Finite element computations and Bloch wave theory are used in this work as they have been proven effective in characterizing the elastic wave propagation characteristics in periodic cellular solids and architectures [15, 16, 18, 19]. In addition, they allow for accurately representing the geometric and topological features of commercially available honeycomb.

The finite element-Bloch wave theory based methodology, which is explained next, is used to conduct two parallel investigations. The first aims to determine the acoustic characteristics of the double-sided hexagonal honeycombs that are commonly used in composite sandwich structures designed for aerospace and marine applications. For this end, multiple realistic, double-sided, and industry relevant honeycomb geometries are analyzed. These geometries are discussed in details in this chapter. The second investigation aims to shed light on the effect of the dominant deformation mechanisms in cellular solids on their acoustic properties. For this end, single sided hexagonal and triangular cells, representing the two main deformation mechanisms (i.e., bending-dominated and stretching-dominated deformation modes), are analyzed.

In the following, the models used in investigating the acoustic properties in commercially available double sided honeycombs is discussed first. Subsequently, the models used to investigate the effect of deformation modes is described. Finally, the computational implementation of Bloch wave theory in finite element models is discussed.

3.1. Models of Double-sided Honeycombs

Aluminum honeycomb cores used in sandwich structures are mostly made by bonding thin corrugated aluminum sheets as illustrated in Figure 3.1. For such honeycombs, two thirds of their cell walls have the same thickness as that of the

corrugated aluminum sheets, while the remaining one third have double the corrugated sheets' thickness. Honeycombs with such configuration are often called double walled honeycombs. The non-uniformity in cell wall thickness for double walled honeycombs affects their deformation mechanisms and increases their elastic anisotropy [3]. The latter, and since elastic wave propagation in a medium depends on its elastic behavior, renders wave propagation in double sided honeycombs more anisotropic than in their single sided counterpart.

One of the most commonly used double sided aluminum honeycombs in sandwich structures tailored for aerospace and marine applications is the honeycombs family made by Hexcel Corporation. Owing to its wide use in the sandwich structure industry, this family of double sided honeycombs is selected for this study and is used as a representative of the commercially available aluminum honeycomb cores. Double sided honeycombs offered by Hexcel vary in their cell size, cell wall thickness, and relative density to satisfy the needs of the sandwich structures industry. 18 different honeycombs that cover the wide range of honeycombs offered by Hexcel are used in this work. The wave propagation characteristics in each of the 18 honeycombs are computationally investigated. The geometric properties and relative density (i.e., two dimensional areal density) of the 18 investigated honeycombs are listed in Table 1.

Aluminum sheets used to make the 18 selected honeycombs are assumed to have isotropic elastic properties, a young's modulus (E) of 70 GPa, a Poisson's ratio (ν) of 0.33, and a density (ρ) of 2700 Kg/m^3. These properties are representative of most aluminum alloys and follow the specifications included in the honeycombs' product data sheets, which are available on the website of the manufacturer. The out-of-plane thickness of the honeycombs can vary. However, as this work is focused on the in-plane wave propagation in the double sided honeycombs, the 18 analyzed honeycombs are assumed to have an out-of-plane height of unit length.

3.2. Models of Stretching and Bending Dominated Honeycombs

The two lattices analyzed in this study are shown in Figures 3.2 and 3.3. A hexagonal honeycomb, which is bending dominated, is shown in Figure 3.2. Hexagonal honeycomb is proven to deform mostly by the bending of its ligaments [3].

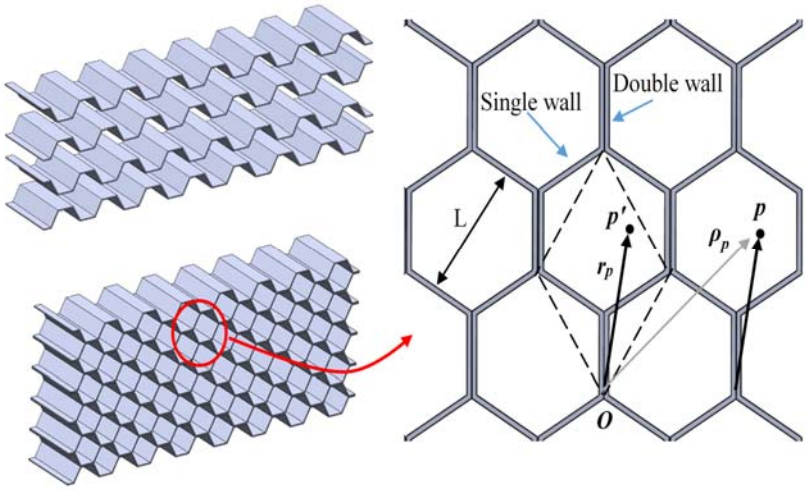

Figure 3.1: Fabrication of honeycombs by bonding of corrugated aluminum sheets, showing: the corrugated sheets (top left), 3D view of the resulting honeycomb (bottom left), and a two dimensional view of the resulting honeycomb (right). The latter shows that each cell has cell walls with twice the thickness of the sheet. Dashed lines in the right figure are the borders of the representative unit cell for this honeycomb.

Table 1. Geometric properties of the investigated double sided aluminum honeycombs

Case	Cell size (L) (inch)	Cell thickness (inch)	% Relative density	Case	Cell size (inch)	Cell thickness (inch)	% Relative density
1	0.0625	0.0007	3.0	10	0.1875	0.0015	2.1
2	0.0625	0.0015	6.4	11	0.1875	0.0025	3.6
3	0.125	0.0007	1.5	12	0.25	0.0007	0.7
4	0.125	0.0015	3.2	13	0.25	0.0015	1.6
5	0.125	0.003	6.4	14	0.25	0.0025	2.7
6	0.15625	0.0007	1.2	15	0.375	0.0007	0.5
7	0.15625	0.0015	2.6	16	0.375	0.0015	1.1
8	0.15625	0.0025	4.3	17	0.375	0.0025	1.8
9	0.1875	0.0007	1.0	18	0.375	0.005	3.6

For instance, under uniaxial loading, the elastic strain energy stored in the ligaments of a hexagonal honeycomb is comprised of mainly bending strain energy (more than 95%) and an insignificant amount (5%) of axial strain energy [8, 9]. Figure 3.3 shows the stretching dominated lattice analyzed in this work. It is derived from the regular honeycomb shown in Figure 3.2 and it has most of the attributes of a periodic honeycomb, but it also includes internal reinforcing ligaments. The extra ligaments bring its nodal connectivity (i.e., number of ligaments intersecting a node) to 6. This is the threshold after which 2D periodic lattices with uniform nodal connectivity act in a

stretching dominated manner regardless of their loading conditions [8, 9, 34]. So under any arbitrary load, the ligaments of the lattice in Figure 3.3 will develop negligible internal bending moments. Both used honeycomb-based lattices (regular and reinforced) are assumed to have high porosity (>95%) as well as slender and prismatic ligaments; therefore, shear stress in their ligaments can be ignored [3]. High porosity level is considered in this work as most honeycomb-like materials used in engineering applications have very high porosity [33].

Throughout this work, and similar to the former section, lattices' ligaments are assumed to have a length of 2.5 mm and to be made of isotropic aluminum with a density of 2700 kg/m^3, a Poison's ratio of 0.33, and a Young's modulus of 70 GPa. As in-plane wave propagation is considered in this work, the out-of-plane dimension of the lattices' ligaments is set to the practical value of unit length. Moreover, lattices of Figures. 3.2 and 3.3 are analyzed using three porosity levels. The latter aims to determine the effect of porosity on the dispersive and direction dependent phase velocities in bending and stretching dominated lattices. However, porosity is represented in this work as relative density, ρ^*, which is defined as the ratio of the unit cell's density to the constituent material density. Accordingly, the relative density of the honeycomb (Figure 3.2) and the reinforced honeycomb (Figure 3.3) are $\rho^* = \frac{2t}{\sqrt{3}L}$ and $\rho^* = \frac{8t}{\sqrt{3}L}$, respectively. Here t and L represent the thickness and length of the lattices' ligaments, respectively. The three relative densities, ρ^*, used in this work are 0.5%, 1.0%, and 1.5%, and for each relative density, three different cell sizes were considered, resulting in 18 different case for both lattices. The geometric properties and relative density (i.e., two dimensional areal density) of the investigated lattices are listed in Table 2.

3.3. Finite Element Model and Bloch Theory Implementation

Bloch wave theory was originally used in the fields of solid state physics to describe the wave propagation of electrons and phonons in solid materials with crystalline and periodic atomic structures. A detailed description of the theory is included in Brillouin [6]. In general, Bloch wave theory allows for expressing the periodic behavior of a wave, including its dispersive and attenuative behaviors, across solid materials with spatially periodic heterogeneities. Thus, it is often used as a homogenization tool to describe the wave propagation characteristics in periodic and

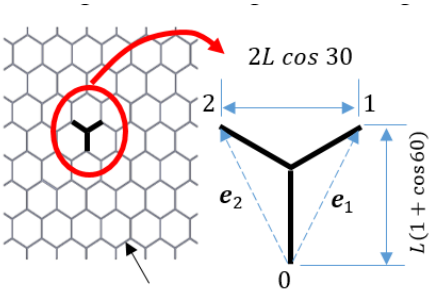

Figure 3.2: Hexagonal honeycomb lattice. Showing the periodic structure (left) and the corresponding unit cell (right) with its basis vectors (dashed lines)

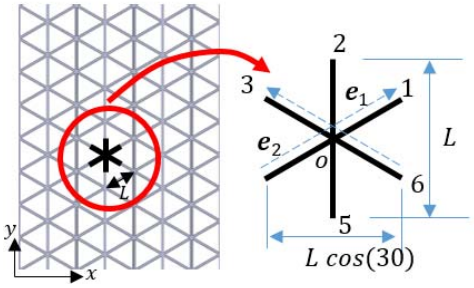

Figure 3.3: Reinforced honeycomb lattice. Showing the full structure (left) and the corresponding unit cell (right) with its basis vectors (dashed lines)

Table 2. Geometric properties of both single-sided hexagonal and triangular lattices

Case	Cell size (L) (mm)	% Relative density
1	2.5	0.5
2	2.5	1.0
3	2.5	1.5
4	5.0	0.5
5	5.0	1.0
6	5.0	1.5
7	10	0.5
8	10	1.0
9	10	1.5

heterogeneous mediums [15, 16, 18, 19], such as the periodic double-walled and triangular honeycombs considered in this study.

In this work, Bloch wave theory is used in conjunction with finite element analysis following multiple efforts that used similar approach to characterize wave propagation in various cellular architectures [14, 15, 38]. Bloch wave theory is used, in particular, to define the periodic boundary conditions that should be applied on representative volume elements (i.e., unit cells) that effectively represent the investigated cellular architectures. The representative unit cells represent all the important features of their parent honeycomb, and repeating them periodically reproduces their parent architecture. The periodic boundary conditions defined using Bloch wave theory implicitly represent the effective (i.e., homogenized) dispersive and attenuative behavior of the honeycomb. The unit cell along with the periodic boundary

conditions are analyzed using finite element method and results are used to describe the wave propagation in the investigated honeycomb architectures. The aforementioned overview is explained in details next.

The implementation of Bloch theory in finite element analysis starts with selecting representative unit cells of the structures analyzed. Three main cellular structures are considered in this work: double sided honeycomb, single sided honeycomb, and triangular honeycomb. The representative unit cell selected to model the double sided honeycombs is shown in Figure 3.1. Evidently, periodically repeating the selected unit cell reproduces the overall periodic double-sided honeycomb structure. The unit cell is also shown in Figure 3.4 along with its lattice basis vectors ($\boldsymbol{e}_1, \boldsymbol{e}_2$), which are used to represent any point inside the unit cell. The lattice vectors are the directions along which the unit cell should be periodically replicated to reproduce the original parent structure. To derive the periodic boundary conditions, arbitrary point P' and its periodic image P are introduced in Figure 3.1. The spatial location of point P in the honeycomb can be described using

$$\rho_p(n_1, n_2) = \boldsymbol{r}_p + n_1\boldsymbol{e}_1 + n_2\boldsymbol{e}_2 \tag{1}$$

such that $\boldsymbol{r}_p$ is the position of the point P in the reference unit cell (i.e., P' in Figure 3.1) and ρ_p is the position of point P in a cell located at n_1 and n_2 cells away from the reference unit cell. n_1 and n_2 can only take integer values. When a sinusoidal in-plane displacement wave propagates in the periodic structure of Figure 3.1 from point O to point P', it can be described at P' as

$$\boldsymbol{u}(\boldsymbol{r_p}) = \boldsymbol{u}_o e^{i\omega t + \boldsymbol{k}.\boldsymbol{r}_p} \tag{2}$$

such that $\boldsymbol{u}_o$ and ω are the wave amplitude and angular frequency observed at the reference point O in Figure 3.1. $\boldsymbol{k}$ is the two dimensional wave vector representing the dispersion and attenuation in the material and $\boldsymbol{r}_p$ is the position vector locating point P' in the reference cell. Assuming $\boldsymbol{k}$ is constant across the honeycomb, then the wave arriving at point P in cell (n_1, n_2) can be described as

$$\boldsymbol{u}(\boldsymbol{\rho_p}) = \boldsymbol{u}(\boldsymbol{r_p})e^{\boldsymbol{k}.(\boldsymbol{\rho_p}-\boldsymbol{r}_p)} = \boldsymbol{u}(\boldsymbol{r_p})e^{\boldsymbol{k}.(\boldsymbol{n_1e_1}+\boldsymbol{n_2e_2})} \tag{3}$$

To simplify the aforementioned equations, the wave vector, $\boldsymbol{k}$, is represented in the reciprocal space defined using the vectors $\boldsymbol{b}_1$and $\boldsymbol{b}_2$ as follows

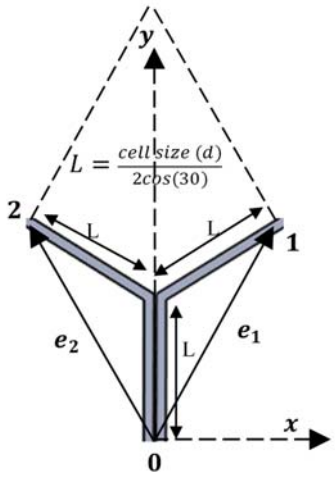

Figure 3.4:. Representative unit cell used to model the double walled honeycomb. $\boldsymbol{e_1}$ and $\boldsymbol{e_2}$ are the lattice basis vectors.

$$\boldsymbol{k} = \boldsymbol{2\pi/\lambda} = k_1\boldsymbol{b}_1 + k_2\boldsymbol{b}_2 = \xi_1\hat{\boldsymbol{\imath}} + \xi_2\hat{\boldsymbol{\jmath}} \tag{4}$$

such that the reciprocal vectors are defined using the condition $\boldsymbol{b_i}.\boldsymbol{e}_j = \delta_{ij}$; $\boldsymbol{\lambda}$ is the wave length vector; k_1 and k_2 are the components of the wave vector in the reciprocal space; ξ_1 and ξ_2 are the components of the wave vectors in the Cartesian coordinate system; $\hat{\boldsymbol{\imath}}$ and $\hat{\boldsymbol{\jmath}}$ are the orthonormal unit vectors representing the Cartesian coordinate system. From Eqns. (3) and (4), the displacement at point *P* in cell (n_1, n_2) can be described as

$$\boldsymbol{u}(\boldsymbol{\rho_p}) = \boldsymbol{u}(\boldsymbol{r_p})e^{\boldsymbol{k}.(\boldsymbol{n_1e_1+n_2e_2})} = \boldsymbol{u}(\boldsymbol{r_p})e^{k_1\boldsymbol{n_1}+k_2\boldsymbol{n_2}} \tag{5}$$

applying this equation to the representative unit cell leads to the following periodic boundary conditions

$$\boldsymbol{u}_1 = \boldsymbol{u}_0e^{k_1},\ \boldsymbol{u}_2 = \boldsymbol{u}_0e^{k_2} \tag{6}$$

such that the displacements $\boldsymbol{u_0}$, $\boldsymbol{u_1}$, and $\boldsymbol{u_2}$ are the displacements at points 0, 1, and 2 shown in Figure 3.4, which are the boundary points of the representative unit cell. Equation (6), through the complex wave vector components k_1 and k_2, accounts for the dispersion and attenuation affecting the wave as it propagates across the unit cell. In this work, the focus is on the dispersive properties of the double walled honeycomb, which are caused by the topological features of the honeycomb. Aluminum used in honeycombs is linear elastic and exhibits negligible material damping at room temperature. Thus, attenuation in aluminum honeycombs due to viscous effects (i.e.,

friction and thermal loss) is negligible. To account only for the dispersive behavior, the complex wave vector components k_1 and k_2 are assumed to have imaginary components only [14].

Before applying the periodic boundary conditions to the unit cell, the cell walls of the unit cell are discretized into nodes and beam elements using the finite element method. For the discretized unit cell, the dynamic equilibrium equation under force-free vibrations is

$$([\boldsymbol{K}] - \boldsymbol{\omega^2}[\boldsymbol{M}])[\boldsymbol{u}] = \boldsymbol{0},\ [\boldsymbol{u}] = [\boldsymbol{u_o}, \boldsymbol{u_1}, \boldsymbol{u_2}, \boldsymbol{u_i}]^{\boldsymbol{T}} \tag{7}$$

where $[\boldsymbol{K}]$is the stiffness matrix, $[\boldsymbol{M}]$ is the mass matrix, $[\boldsymbol{u}]$ is the displacement at the nodes, and $\boldsymbol{u_i}$ refers to the displacements of the internal nodes of the unit cell (i.e., the ones not exposed to the boundary conditions). To account for dispersion in Eqn. (7), the periodic boundary conditions represented by Eqn. (6) are incorporated. Using Eqn. (6) in Eqn. (7) and applying static condensation to reduce the size of the system result in

$$[\bar{\boldsymbol{K}} - \omega^2 \bar{\boldsymbol{M}}] \begin{bmatrix} \boldsymbol{u_o} \\ \boldsymbol{u_i} \end{bmatrix} = [\boldsymbol{0}] \tag{8}$$

such that $[\bar{\boldsymbol{K}}]$ and $[\bar{\boldsymbol{M}}]$are the reduced stiffness and mass matrices, respectively. They are functions of the original stiffness and mass matrices as well as the wave numbers k_1 and k_2. Equation (8) is an Eigenvalue problem that can be solved to find the Eigenfrequencies and Eigenvectors. The unknowns in Eqn. (8) are the wave vectors, k_1 and k_2, and the frequency ω. Accordingly, to solve Eqn. (8), the wave vectors k_1 and k_2 are prescribed first, and then the Eigenfrequencies $\boldsymbol{\omega}$ (k_1, k_2) corresponding to them are determined.

In this work, Eqn. (8) is solved using the finite element software ABAQUS. Each of the cell walls of the unit cell is discretized using 50 two-node Euler beam elements (B21 elements per ABAQUS terminology). Euler beam is chosen as honeycomb's cell walls are too thin and transverse shear stress in them is ignorable [3, 14]. The selected number of elements per cell wall are chosen as earlier studies regarding mesh sensitivity and mesh effect on the wave propagation in regular honeycombs and triangular structures showed that 50 elements per cell ensure mesh independence[14]. The periodic boundary conditions, Eqn. (6), are incorporated in

ABAQUS as equations using the ABAQUS equation command. These equations include the prescribed values of k_1 and k_2. Both the stiffness and mass matrices are internally assembled by the software, following standard finite element and Euler beam theories. Finally, the eigenvalue problem represented by Eqn. (8) is solved for the Eignvalues $\boldsymbol{\omega}$ using the Lanczos Eigensolver in ABAQUS. This process is repeated for multiple values of (k_1, k_2) which results in the dispersion surfaces $\boldsymbol{\omega} = \boldsymbol{\omega}(k_1, k_2)$. Dispersion surfaces are then used to compute the phase velocities. To determine the full dispersion surfaces, k_1 and k_2 are varied according to Bloch's theorem in the first Brillouin zone [6, 14, 15]. This zone is presented in Figure 3.5 and represents the periodicity of the structure in the reciprocal space. The phase velocities are then obtained from the dispersion surfaces using $\boldsymbol{v} = \omega/\boldsymbol{k}$. Results obtained from this approach are presented next.

The outlined approach in itself is straightforward and well-established [14-16, 38]. However, the implementation of the approach should be verified. For this end, the current implementation of the outlined approach was tested first on two honeycomb structures with uniform cell wall thickness (i.e., not double sided) and dimensions identical to honeycombs analyzed in two different studies [14, 38]. Results from the verification tests were compared to the published ones in terms of Brillouin zone dimensions, dispersion surfaces, and phase velocities. Comparisons underscored a total agreement between the verification tests and the published data.

The methodology so far emphasized on the approach used to investigate the acoustic behavior of double-honeycombs. The same approach was used to investigate the effect of deformation mechanisms in hexagonal and triangular based honeycombs. So, two unit cells were created. The first represented a single-sided hexagonal honeycomb and is shown in Figure 3.2, while the second represented a single-sided triangular honeycomb and is shown in Figure 3.3. The lattice vectors for each of the unite cells are also shown in Figures. 3.2 and 3.3. The unit cell and analysis procedure associated with the single-walled unit cell are identical to the ones developed for the double-sided honeycombs. The only difference is that the thickness of the vertical cell wall in the double-sided honeycomb would be double of the thickness of the vertical wall in its single-sided counterpart. However, for the triangular honeycomb, the

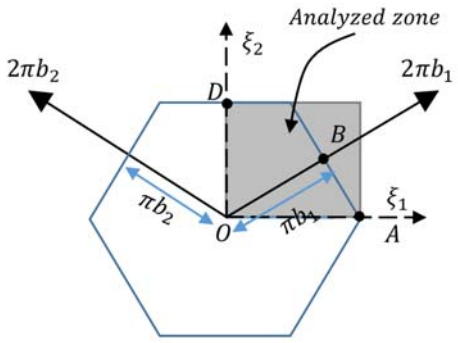

Figure 3.5: First Brillouin zone for the double sided honeycomb. With the symmetry of the 1st Brillouin zone, only the representative shaded region is considered in the analysis.

application of Bloch wave theory would result in different boundary conditions than those represented by Eqn. (6)

The lattice vectors of the triangular unit cell, which are shown in Figure 3.3 as dashed arrows, are defined in terms of the ligament length, L, as $\boldsymbol{e}_1 = L\,cos(30)\hat{\boldsymbol{\imath}} + L\,sin(30)\hat{\boldsymbol{\jmath}}$ and $\boldsymbol{e}_2 = -L\,cos(30)\hat{\boldsymbol{\imath}} + L\,sin(30)\hat{\boldsymbol{\jmath}}$ for the reinforced honeycomb. Applying Bloch theorem, following the same procedure outlined above, to the unit cell of Figure 3.3 results in the periodic boundary conditions

$$\boldsymbol{u}_1 = \boldsymbol{u}_4 e^{k_1}, \boldsymbol{u}_3 = \boldsymbol{u}_6 e^{k_2}, \boldsymbol{u}_2 = \boldsymbol{u}_5 e^{(k_1+k_2)}$$
$$\boldsymbol{f}_1 = -\boldsymbol{f}_4 e^{k_1},\ \boldsymbol{f}_3 = -\boldsymbol{f}_6 e^{k_2}, \boldsymbol{f}_2 = -\boldsymbol{f}_5 e^{(k_1+k_2)} \tag{9}$$

where $\boldsymbol{u}_0$ to $\boldsymbol{u}_6$ and $\boldsymbol{f}_0$ to $\boldsymbol{f}_6$ are the degrees of freedom and the external forces corresponding to the ligaments' boundaries which are named points 0,1, 2, 3, 4, 5, and 6 in Figure 3.3. Once more, k_1 and k_2 are the complex wave numbers along the reciprocal lattice directions $\boldsymbol{b}_1$ and $\boldsymbol{b}_2$, respectively. Following the same reasons outline above for the case of the double-sided honeycomb, the real components of k_1 and k_2 are ignored. Applying the periodic boundary conditions corresponding to Figure 3.3 (i.e., Eqn. (9)) in Eqn. (3) results in the following

$$[\bar{\boldsymbol{K}} - \omega^2 \bar{\boldsymbol{M}}] \begin{bmatrix} \boldsymbol{u_4} \\ \boldsymbol{u_5} \\ \boldsymbol{u_6} \\ \boldsymbol{u_i} \end{bmatrix} = [\boldsymbol{0}] \tag{10}$$

where $\boldsymbol{u_4}$, $\boldsymbol{u_5}$, and $\boldsymbol{u_6}$ are the degrees of freedom of the independent boundary nodes shown in Figure 3.3. Again $\boldsymbol{u_i}$ represents the internal degrees of freedom. Equation

(10) is an Eigenvalue problems that govern the free vibration behavior of the unit cell, and it implicitly account for the dispersive and direction dependent properties of the lattices. Dispersion and direction dependence are represented through the dependence of ω on the wave numbers k_1 and k_2. To solve Eqns. 10, the wave numbers k_1 and k_2 are prescribed values, and subsequently the equations are solved for the Eigenfrequency $\omega(k_1,k_2)$. The range of k_1 and k_2 covered is bounded by the lattices' 1st Brillouin zone [6]. This zone represents the periodicity of a lattice in its reciprocal space and comprises the wave vector range needed to fully characterize its dispersion properties [14, 16, 33, 39, 40]. The 1st Brillouin zone of the triangular honeycomb lattice is shown in Figure 3.6. Due to the symmetry of the 1st Brillouin zone, only the first quadrant, which is highlighted in Figure 3.6, is used. Utilizing symmetry allows for predicting the results corresponding to the other three quadrants. Each point in the 1st Brillouin zone represents a wave vector, $\boldsymbol{k}$, that can be expressed using the reciprocal lattice directions, $\boldsymbol{b}_1$ and $\boldsymbol{b}_2$, or using the Cartesian coordinate system, $\hat{\boldsymbol{\imath}}$ and $\hat{\boldsymbol{\jmath}}$. To transform $\boldsymbol{k}$ back-and-forth between the two coordinate systems, the relation $\boldsymbol{k} = k_1\boldsymbol{b}_1 + k_2\boldsymbol{b}_2 = \xi_1\hat{\boldsymbol{\imath}} + \xi_2\hat{\boldsymbol{\jmath}}$ is used. Here ξ_1 and ξ_2 are the components of $\boldsymbol{k}$ in the Cartesian coordinate system. Results of the finite element based approach describe the variation of the first two Eigenfrequencies (ω_1, ω_2) with the wave vector, $\boldsymbol{k}$, over the wave vector range defined by the lattices' 1st Brillouin zone. The Eigenfrequencies obtained from this analysis are then processed to compute the phase velocities using the relation $\boldsymbol{v} = \omega/\boldsymbol{k}$ [16, 39]. Thus, in summary, this approach determines the Eigenfrequencies, $\boldsymbol{\omega}$, and phase velocity, $\boldsymbol{v}$, corresponding to a range of wave vectors.

The aforementioned derivation of Eqns. (8) and (10) serves as a theoretical background to help understand the approach and results. However, in this work these equations are generated and solved automatically in ABAQUS using its Eigenfrequency solver. The implementation in ABAQUS involves four steps: discretizing the ligaments of the unit cells using 50 beam elements, assigning values to the components of the wave vector k_1 and k_2, applying the periodic boundary conditions (Eqns. 6 and 9) using the EQUATION command, and finally solving for the first two Eigenfrequencies using ABAQUS's Lancosz Eigenfrequency solver. The process is repeated for the range of k_1 and k_2 values bound by the lattices' 1st Brillouin zone. Only the first two Eigenfrequencies are obtained as they are the most

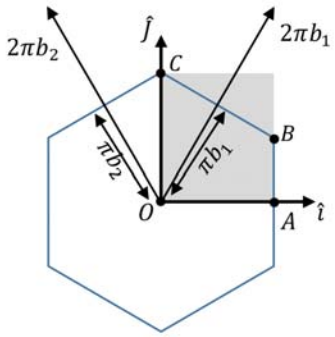

Figure 3.6: 1st Brillouin zone associated with the unit cell of the honeycomb-like structure. $\hat{\imath}$ and $\hat{\jmath}$ are the unit vectors aligned with the *x* and *y*-axes, respectively

fundamental. The first Eigenfrequency corresponds to an asymmetric (i.e., shear) propagating wave and the second Eigenfrequency corresponds to a symmetric (i.e., longitudinal) propagating wave [38].

Chapter 4. Results

This chapter is divided into two sections. The first section reports on the acoustic characteristics, in terms of dispersion surfaces and velocity profiles, of commercially available double-sided aluminum hexagonal honeycombs. On the other hand, the second section presents the results of the finite element computations investigating the effect of the dominant deformation mechanism (i.e. stretching or bending) in cellular architectures on their acoustic characteristics.

4.1 Acoustic Characteristics of Double-sided Hexagonal Honeycomb

The number of eigenvalues corresponding to Eqn. (8) is equal to the rank of the reduced stiffness $[\bar{\boldsymbol{K}}]$ and mass $[\bar{\boldsymbol{M}}]$ matrices as well as the number of independent degrees of freedom comprising $\boldsymbol{u_o}$ and $\boldsymbol{u_i}$. Thus, for the unit cell analyzed in this work, which is modeled using 50 two dimensional beam elements per cell wall and has 447 degrees of freedom upon the application of the periodic boundary conditions, i.e., a total of 447 Eigen frequencies can be obtained. However, only the first and second Eigenfrequencies are computed here as they are associated with the two fundamental in-plane wave propagation modes, namely the antisymmetric and symmetric modes. In particular, the first Eigenmode is the antisymmetric mode and is associated with shear elastic waves, while the second Eigenmode is the symmetric mode and is associated with longitudinal elastic waves [38].

To ensure that the first two modes obtained are the antisymmetric and symmetric ones, the deformed configurations corresponding to the first two modes were determined and checked for every analyzed case as well as for different k_1, k_2 values. For illustration purposes, the deformed configurations corresponding to the first two modes for case 1 and for the k_1, k_2 values marked by points A, B, and D in Figure 3.5 are presented in Figure 4.1. In this figure, only four complete hexagonal cells are plotted and their deformations are scaled up using the factors included in the figure to improve visibility. Figure 4.1 shows that the deformed configurations corresponding to the first modes for the three wave vector values (A, B, and D) are asymmetric and exhibit common features. Asymmetrical deformation causes every two cell walls facing each other to deform in an identical manner as can be observed in Figure 4.1.

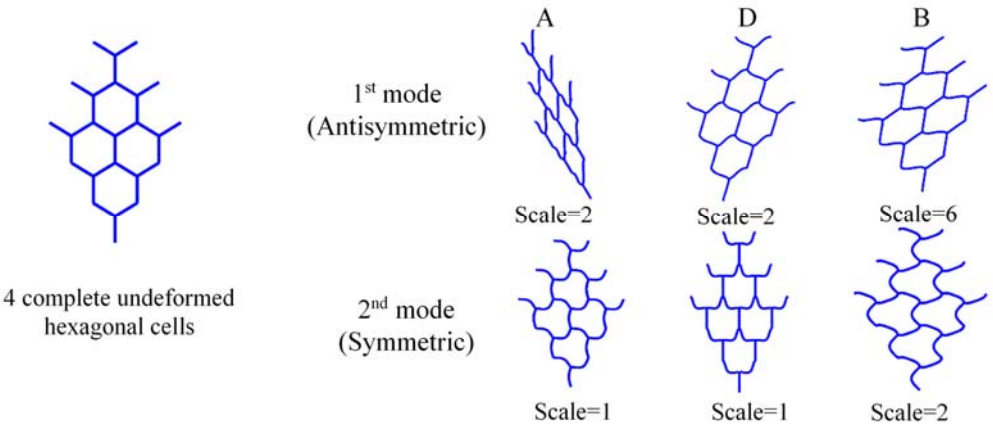

Figure 4.1: First and second Eigenmodes. Showing the deformation according to the modes corresponding to points A, B and D in Figure 3.15. The Figure shows four complete hexagonal cells (deformed and undeformed). Deformations are scaled by the shown factors to enhance visibility

On the other hand, Figure 4.1 shows that the deformation patterns corresponding to the second modes are symmetric. The plane of symmetry for each of the shown 2nd mode deformation patterns is aligned with the direction of the wave vector (i.e., points A, B, and D in Figure 3.5).

For each of the 18 cases listed in Table 1, the first two Eigenfrequencies are obtained for the range of k_1, k_2 values defined by the 1st Brillouin zone. Resulting frequencies are used to construct the first and second modes dispersion surfaces (i.e., $\omega_1 = \omega_1(k_1, k_2)$ and $\omega_2 = \omega_2(k_1, k_2)$) shown in Figures 4.2 and 4.3, respectively. Due to the symmetry of both of the Brillouin zone and the unit cell, only the first quadrant of the Brillouin zone is considered[14]. Simulations included few k_1, k_2 values that lie outside the Brillouin zone. These points are used to check for the symmetry of the dispersion surfaces; an additional check to ensure the correctness of the analysis. Accordingly, the k_1, k_2 values analyzed are the ones confined by the shaded zone in Figure 3.5.

Dispersion surfaces in Figures. 4.2 and 4.3 are plotted using contour lines. Each line represents the values of $k_1$and k_2 corresponding to a single frequency. These two figures highlight the dispersive nature of double sided honeycombs as well as the frequency range at which double sided honeycombs exhibit direction independent wave propagation characteristics. Non dispersive and acoustically isotropic materials exhibit

dispersion surfaces with circular contours that expand such that the ratio between frequency and contour's radius remains constant. On the contrary, contours in Figure 4.2 are noncircular, even at the smallest computed frequencies (sub kHz). Thus, asymmetric wave propagation in double sided honeycombs always exhibits direction dependent propagation properties that depend on the periodic cellular structure of the honeycomb. On the other hand, Figure 4.3 shows perfect circular contours at lower frequencies. Thus, below a certain frequency, a propagating wave with symmetrical deformation mode can exhibit direction independent behavior. The frequency at which this direction independent behavior commences depends on the relative density, cell size and dimensions of the honeycomb. The range of frequencies with direction independent propagation characteristics, is the one most suited to be used in elastic waves based nondestructive techniques. At higher frequencies, both modes exhibit increased direction dependent characteristics.

Although, Figures 4.2 and 4.3 can be used to describe the dispersive properties of double sided honeycombs, it is more practical to analyze their dispersive behavior using phase velocity plots. Phase velocities are computed for each of the analyzed 18 cases using

$$\boldsymbol{v} = \omega/\boldsymbol{k} \tag{11}$$

where phase velocity is defined as the angular frequency to wave vector ratio[38]. Phase velocities for the asymmetrical and symmetrical deformation modes are presented in Figures 4.4 and 4.5, respectively, but only for the range of frequencies associated with nondispersive to marginally dispersive behavior (i.e., small frequencies associated with circular and semi-circular contours in Figures 4.2 and 4.3). These frequencies correspond to phase velocity contours that negligibly change or contract with increase in wave frequency. The emphasis on these frequencies stems from their potential to be used in the nondestructive inspection of honeycombs. It is important to note that the lowest frequency considered for each case in Figures 4.4 and 4.5 represents the limit below which the response is non-dispersive and frequency independent. To facilitate conducting comparisons, cases in Figures 4.4 and 4.5 are ordered based on their relative density in an ascending manner..

Phase velocities for the first mode (Figure 4.4) shows significant direction dependent behavior, at all frequencies (i.e., acoustically anisotropic).

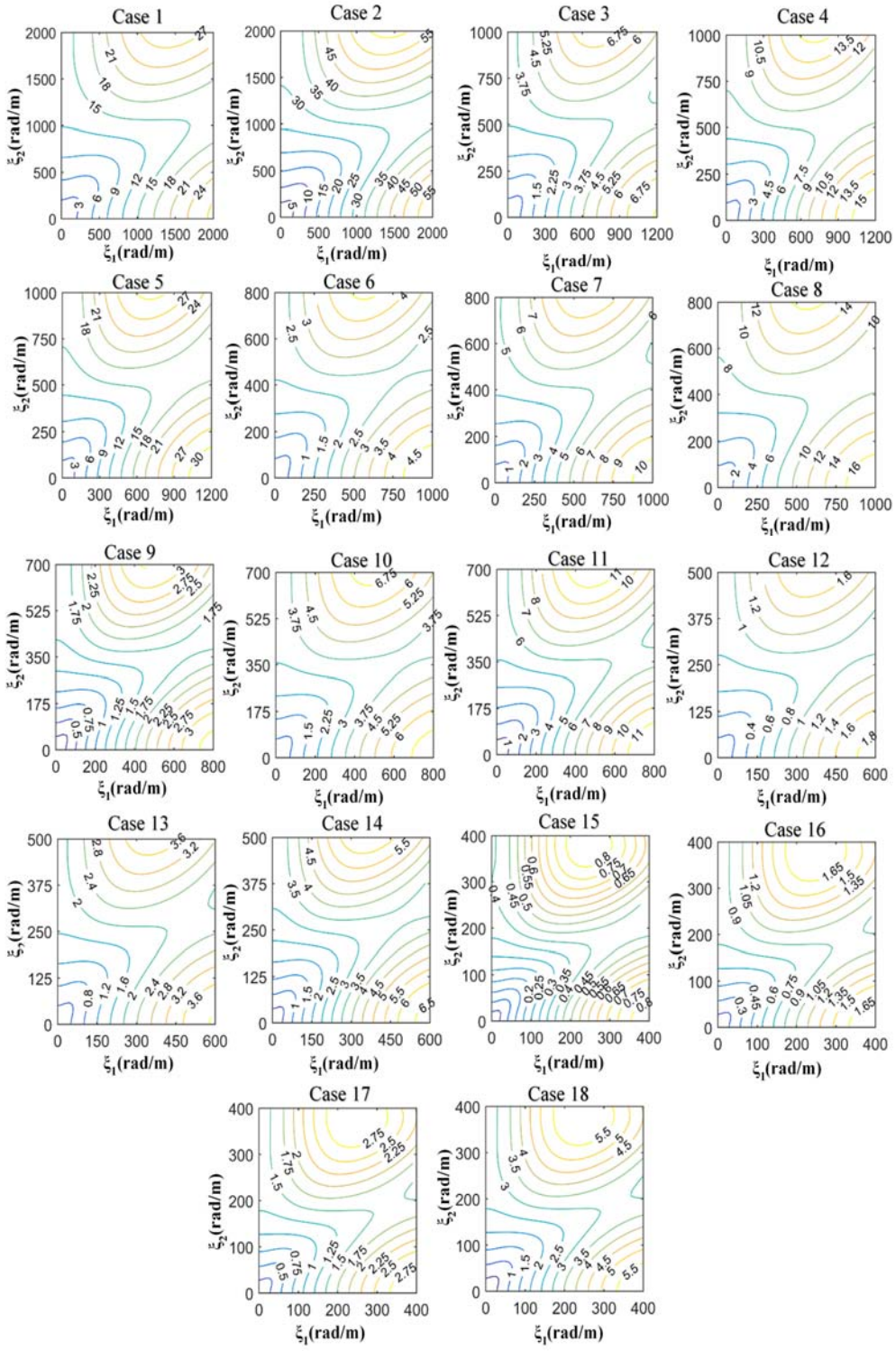

Figure 4.2: Dispersion maps corresponding to the 1st Eigenmode for the 18 cases. Isolines represent the dispersion vectors ($\boldsymbol{k} = \xi_1\hat{\imath} + \xi_2\hat{\jmath}$) corresponding to the same Eigenfrequency, which is shown on the isolines in kHz.

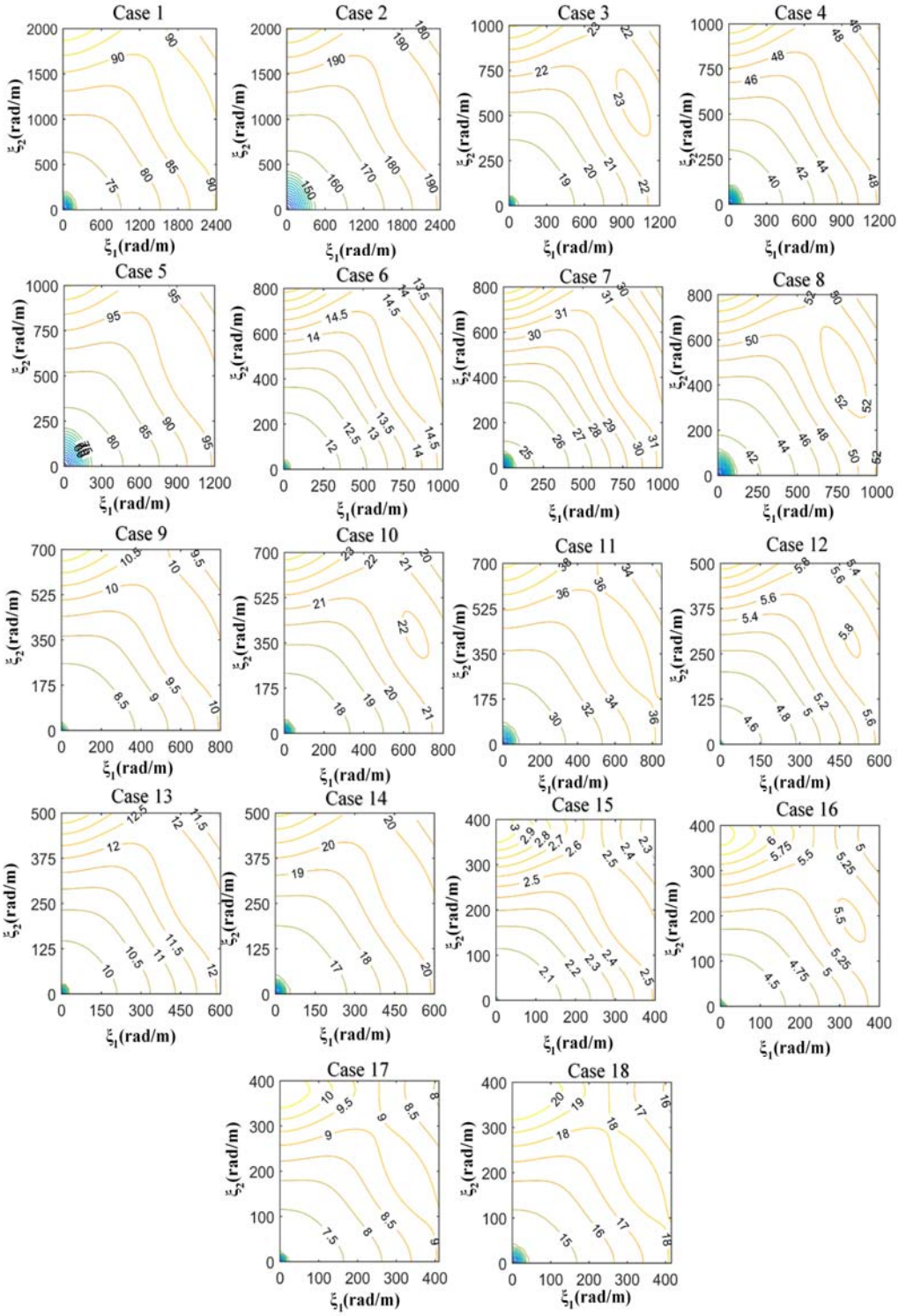

Figure 4.3: Dispersion maps corresponding to the 2nd Eigenmode for the 18 cases. Isolines represent the dispersion vectors ($\boldsymbol{k} = \xi_1\hat{\imath} + \xi_2\hat{\jmath}$) corresponding to the same Eigenfrequency, which is shown on the isolines in kHz.

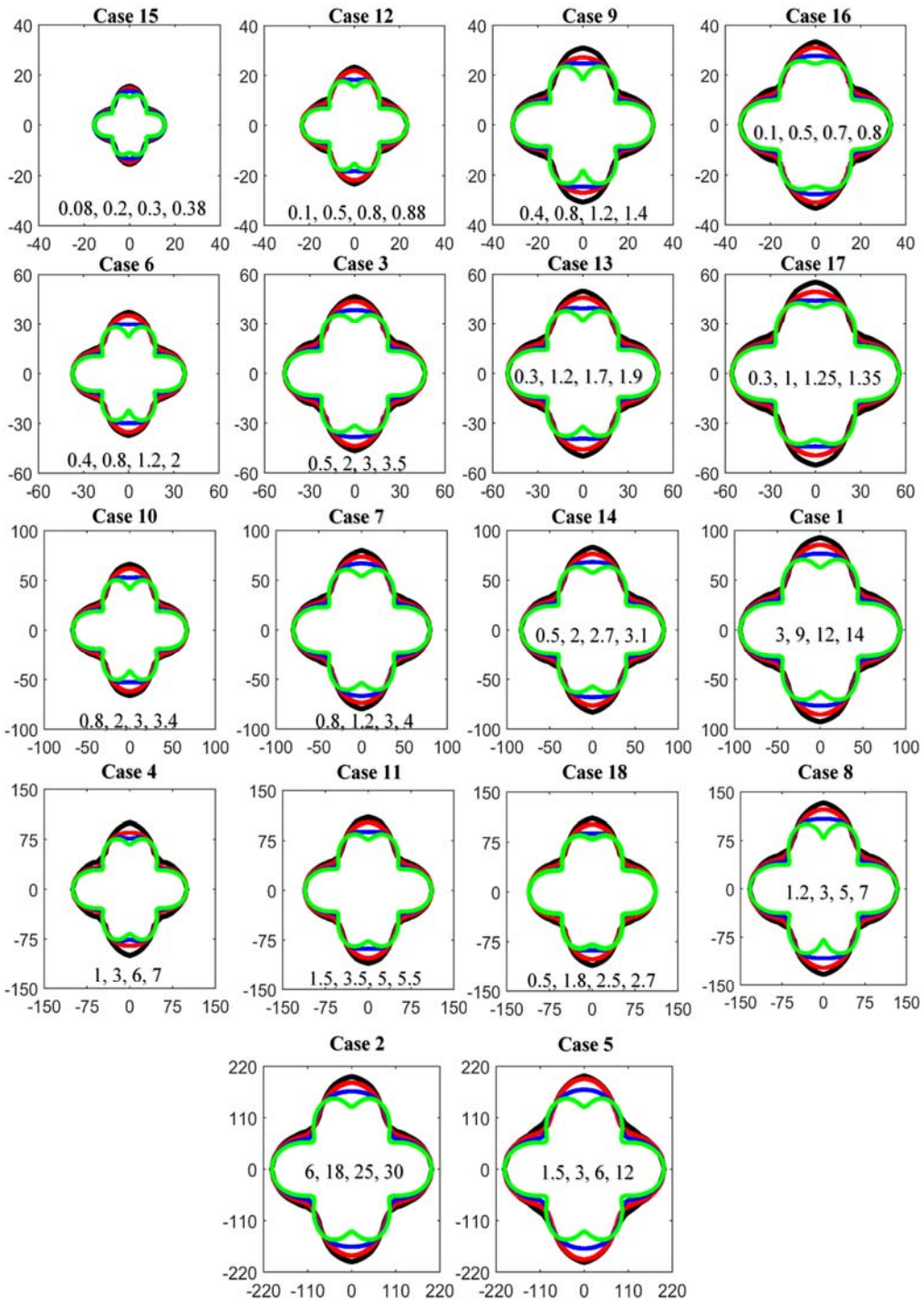

Figure 4.4: First mode phase velocities for the 18 cases. Inserts in the plots represent the frequencies (in kHz) corresponding to the plotted contours; such that the outermost to the innermost contours correspond to the lowest to highest frequencies. Horizontal and vertical axes for all plots represent the phase velocity components (m/s) in the x and y- directions defined in Figure 3.1, respectively.

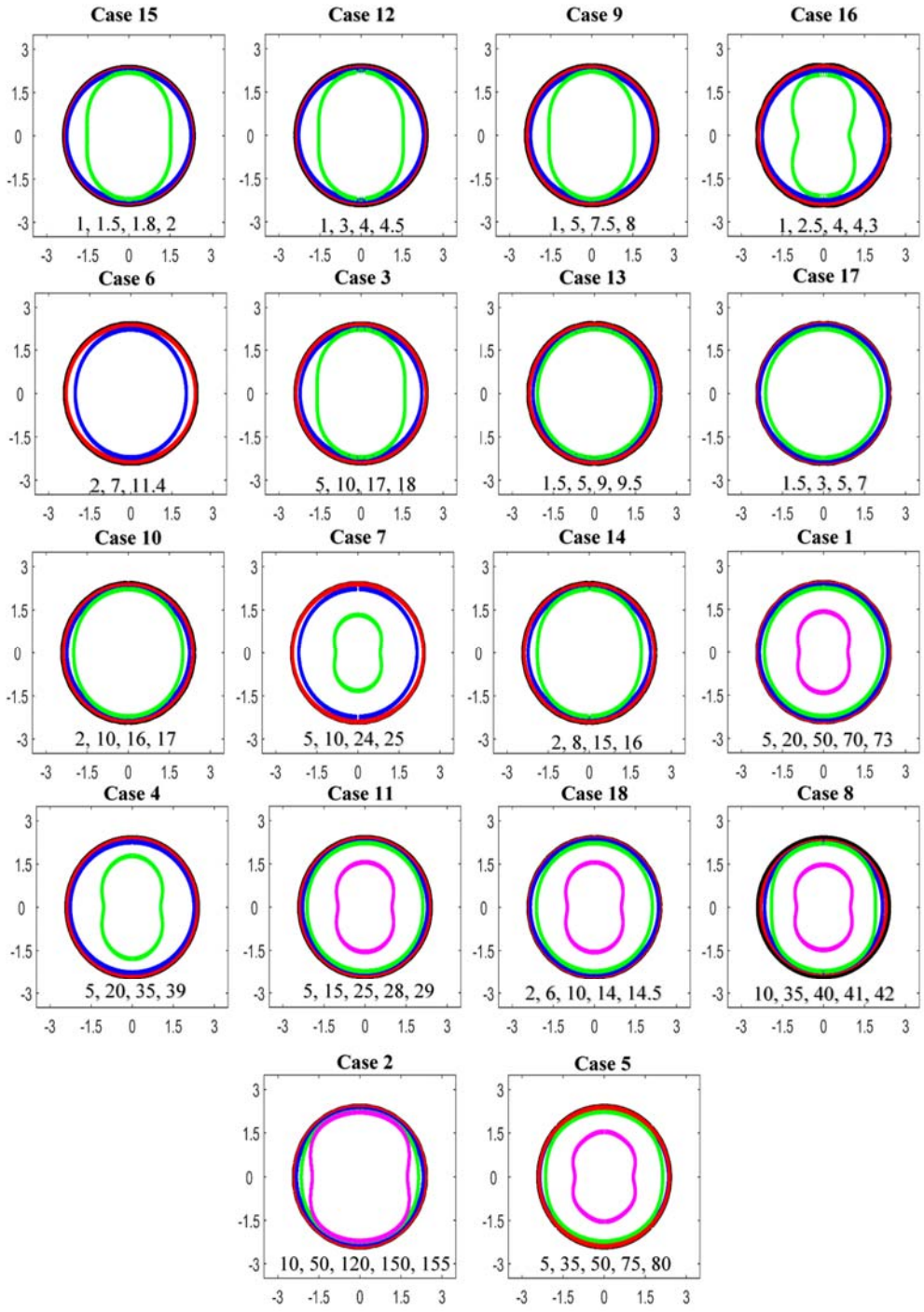

Figure 4.5: Second mode phase velocities for the 18 cases. Inserts in the plots represent the frequencies (in kHz) corresponding to the plotted contours; such that the outermost to the innermost contours correspond to the lowest to highest frequencies. Horizontal and vertical axes for all plots represent the phase velocity components (km/s) along the x and y- directions defined in Figure 3.1, respectively.

As frequency increases, the phase velocity along the y-direction exhibits significant dispersive behavior as well as a decrease in magnitude, while along the x-direction it remains nondispersive. Phase velocities for asymmetrical deformation modes ranged between ~15m/s to ~200m/s which is within the range reported for single wall aluminum honeycombs [14].

Phase velocities for the second mode Figure 4.5 are direction independent and nondispersive at lower frequencies; lower than a cutoff frequency that depends on the periodic structure's parameter (e.g., relative density, cell size and thickness). This is illustrated by the circular velocity contours that preserve their circular shape and size even as the frequency vary by few kHz. However, at higher frequencies the velocity contours distort and change their size indicating directional dependent and dispersive behavior. Nonetheless, for frequencies in the range of 1~100 KHz, there exist, for each case, a range of frequencies at which the symmetrical waves have directional independent and nondispersive behavior. Elastic waves with frequencies from this range can potentially be used in the nondestructive evaluation of honeycomb cores. Also, Figure 4.5 shows that symmetric waves are much faster than their asymmetric counterpart. While asymmetric elastic waves have phase velocities in the range from 15 to 200 m/s depending on the honeycomb case analyzed, symmetric waves have phase velocities that reach ~2400 m/s.

4.2 Effect of Deformation Mechanisms on the Acoustic Properties of Honeycombs

The effect of deformation mechanisms is highlighted through analyzing a bending dominated regular honeycomb lattice and stretching dominated reinforced honeycomb lattice and subsequently comparing their behaviors and properties.

4.2.1 Dispersion surfaces and phase velocities of the regular honeycomb lattice. For the bending dominated honeycomb lattice, the dispersion surfaces corresponding to the eigenfrequencies of its first and second modes are shown in Figures 4.6 and 4.7, respectively. Dispersion surfaces can readily demonstrate the acoustic anisotropy and dispersion properties of periodic lattices. In general, dispersion surfaces with non-circular contours represent direction dependent phase velocities, while circular contours represent direction independent phase velocities. Moreover, non-proportional gradients in the frequency contours with increased wave vector, $\boldsymbol{k}$, magnitude (norm) indicate dispersive behavior. The aforementioned trends are very

clear in the 1st mode dispersion surfaces of the regular honeycomb presented in Figure 4.7. This figure shows circular contours near the origin that transition to noncircular contours at higher wave vector, $\boldsymbol{k}$, magnitudes. This transition occurs, for instance, around 0.75 kHz, 1.5 kHz, and 2.25 kHz for the relative densities 0.5%, 1.0%, and 1.5%, respectively. The latter frequencies represent the limit after which asymmetric waves traversing the honeycomb lattice exhibits direction dependent behavior. Before the direction dependent behavior commences, the contours in Figure 4.7 are proportional to the wave vector, demonstrating non-dispersive behavior. However, upon the onset of the direction dependent behavior, the contours in Figure 4.7 start to non-uniformly space out demonstrating dispersive behavior. Accordingly, for the regular honeycomb, asymmetric propagating waves start to exhibit direction dependent and dispersive behavior at relatively the same transition frequencies. The frequencies at which the transition from non-dispersive and isotropic to dispersive and anisotropic behavior occurs vary proportionally with relative density as seen in Figure 4.7. For instance, increasing the relative density by 2 folds (from 0.5% to 1.0%) and 3 folds (from 0.5% to 1.5%) increase the transition frequency by a factor of 2 (from 0.75 to 1.5 kHz) and 3 (from 0.75 kHz to 2.25kHz), respectively. The effect of relative density on the transition frequencies is part of a larger trend that applies to all frequency contours shown in Figure 4.7. This figure shows that scaling the relative density by a factor of x results in scaling all frequency contours by a factor of x.

Similar to the honeycomb's 1st mode dispersion surfaces, its second mode dispersion surfaces, see Figure 4.7, demonstrate direction independent behavior that transitions to become direction dependent at higher frequencies and large wave vector, $\boldsymbol{k}$, magnitudes. Moreover, contours in Figure 4.7 slowly but not proportionally vary with wave vector, highlighting a significant dispersive behavior. Based on Figure 4.7, the frequencies at which the transition between non-dispersive and isotropic to dispersive and anisotropic behavior occurs around 7 kHz, 14 kHz, and 21 kHz, for the relative densities 0.5%, 1%, and 1.5%, respectively. The contours representing the nondispersive behavior are not easily visible in Figure 4.7 as they have very small radii; however, the range of frequencies associated with the non-dispersive behavior will be highlighted in the subsequent paragraph. Second mode frequency contours in Figure 4.7 mirror the trends observed in Figure 4.6 with respect to dependence on relative density; second mode frequency contours are proportional to relative density.

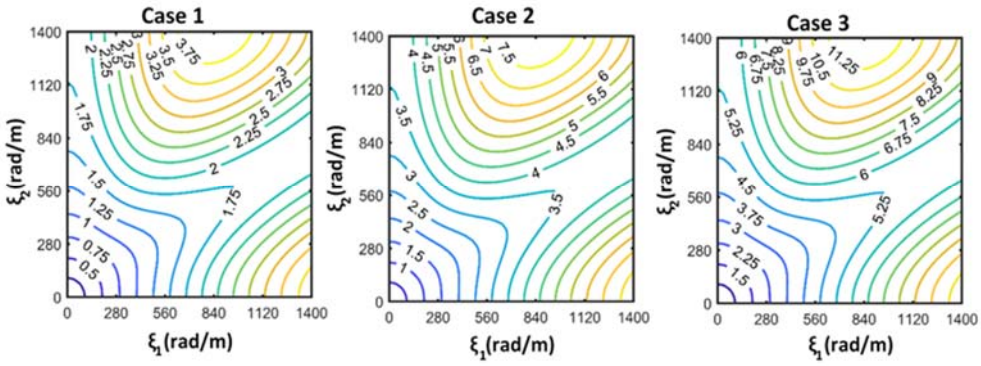

Figure 4.6: Dispersion surfaces corresponding to the 1st Eigenmode of the honeycomb structure. Isolines are in kHz and represent the wave vectors, k, corresponding to the same frequency.

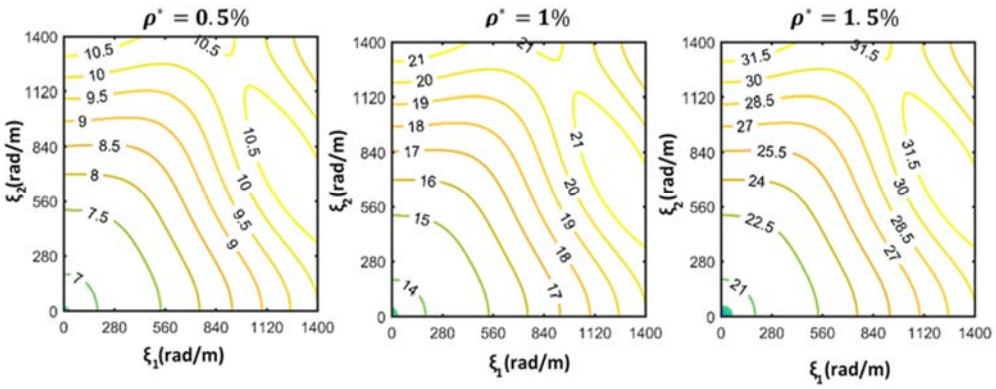

Figure 4.7: Dispersion surfaces corresponding to the 2nd Eigenmode of the honeycomb structure. Isolines are in kHz and represent the wave vectors, k, corresponding to the same frequency.

However, according to Figure 4.7, second mode dispersion surfaces differ from 1st mode dispersion surfaces of Figure 4.6 in that they are less direction dependent; their non-circular contours do not deviate significantly from the circular shape. Thus, longitudinal (symmetric) waves propagating in a regular honeycomb would show less direction dependent behavior as compared to shear (asymmetric) waves.

Another perspective regarding the anisotropic and dispersive behavior of the regular honeycomb is provided through Figure 4.8. This figure is constructed using the data used to plot Figures 4.6 and 4.7, but it shows the variation of the eigenfrequencies (1st mode in Figure 4.8-a and 2nd mode in Figure 4.8-b) with wave vectors aligned with the lattice's material principal directions (i.e., *x* and *y* directions). Accordingly, this figure demonstrates the behavior of asymmetric and symmetric waves propagating

along the material principal directions of the regular honeycomb shown Figure 3.2. Figure 4.8 effectively shows the range of frequencies at which the acoustic response of the honeycomb is non-dispersive and isotropic as well as the transition behavior from the non-dispersive and isotropic phase to the dispersive and anisotropic phase. According to Figure 4.8-a, at each relative density, the relation between the 1st mode eigenfrequency and wave vector magnitude exhibits a linear and direction independent (i.e., isotropic) initial phase. This phase ends at the transition frequencies, which were determined using Figure 4.6, of 0.75 KHz, 1.5 kHz, and 2.25 kHz for the relative densities of 0.5%, 1%, and 1.5%, respectively. Beyond these frequencies, two observations can be seen. First, the relation between 1st mode eigenfrequency and wave vector magnitude becomes nonlinear (i.e., dispersive behavior is present), particularly for waves propagating along the *y*-direction. Second, the behavior of the relation between 1st mode eigenfrequency and wave vector magnitude along the *x* and *y* directions start to progressively deviate, indicating a growing anisotropic behavior at higher frequencies. Figure 4.8-a also shows that the transition process from the non-dispersive and isotropic phase to the dispersive and anisotropic phase is smooth and gradual. With the respect to the 2nd mode eignfrequencies, Figure 4.8-b also demonstrates a transition between a non-dispersive and isotropic behavior to a dispersive and anisotropic behavior. However, the transition is not as smooth as in 1st mode case. The eigenrequency-wave vector plots in Figure 4.8-b exhibit distinct three phases: a non-dispersive, isotropic, and relative density independent initial phase that abruptly ends at the frequencies of 7kHz, 14kHz and 15 kHz for the relative densities of 0.5%, 1%, 1.5%, respectively; a dispersive, isotropic, and relative density dependent second phase that transitions smoothly to the subsequent phase; and a final dispersive, anisotropic, and relative density dependent phase. The second and third phases are apparent in Figure 4.7, but the initial phase is not as it is associated with very small wave vector magnitudes and is practically difficult to show in Figure 4.7. Moreover, in the second and third phases, the 2nd mode eigenfrequency is proportionally dependent on relative density.

The phase velocities corresponding to the honeycomb's 1st and 2nd eigenmodes are computed by applying the relation $\boldsymbol{v} = \omega/\boldsymbol{k}$ to the dispersion surfaces shown in Figures 4.6 and 4.7. To avoid overcrowding the figures, the phase velocities are computed only for few frequencies (i.e., dispersion surfaces' isocontours). These are

selected to allow for illustrating the observed trends per analyzed scenario (i.e., combination of mode, lattice, and relative density). Moreover, efforts were taken to select few overlapping frequencies among the different scenarios, when possible, to highlight the effect of relative density. It is worth mentioning that perfect frequency overlap among the different scenarios is not practically possible due to the limited overlap among the frequency ranges exhibited by the different scenarios. For the regular honeycomb, the phase velocities corresponding to its first and second eigenmodes are shown in Figures 4.9 and 4.10, respectively.

The 1st mode velocity contours, see Figure 4.9, show nondispersive and direction dependent behavior that transitions to become dispersive and direction dependent as already illustrated by the dispersion surfaces. Here, nondispersive behavior manifests as frequency independent velocity contours. For instance, the case with 0.5% relative density shows frequency independent velocity contours at 0.25, 0.5, and 0.75 kHz. At frequencies higher than 0.75 kHz, the contours gradually change shape and size. The change in size underscores frequency dependent behavior, while the deviation from the circular shape represents direction dependent phase velocities. Similar behavior is seen at 1% and 1.5% relative density, but the transition occurs at higher frequencies (1.5 kHz and 2.25 kHz). Phase velocity, based on Figure 4.9, is proportional to relative density. For instance, in the non-dispersive range, a three-fold increase in phase velocity, from 15.77 m/s to 47.31 m/s, is associated with a 3-fold increase in relative density, from 0.5% to 1.5%. The proportional relation between phase velocity and relative density is a result of the proportional dependence of eigenfrequency on relative density, which is illustrated by the dispersion surfaces in Figure 4.9.

Phase velocities corresponding to the 2nd mode of the honeycomb lattice, Figure 4.10, exhibit frequency independent velocity contours with a magnitude of 2550 m/s that sharply transition to become frequency dependent (dispersive). This is consistent with the behavior observed in Figure 4.8-b. For the range of frequencies plotted, phase velocity contours are direction independent. At higher frequencies, based on the dispersion surfaces presented in Figure 4.7, direction dependent velocity contours would be observed. However, including them in Figure 4.10 would be impractical as they would be considerably smaller (not discernable) than the rest of the contours in

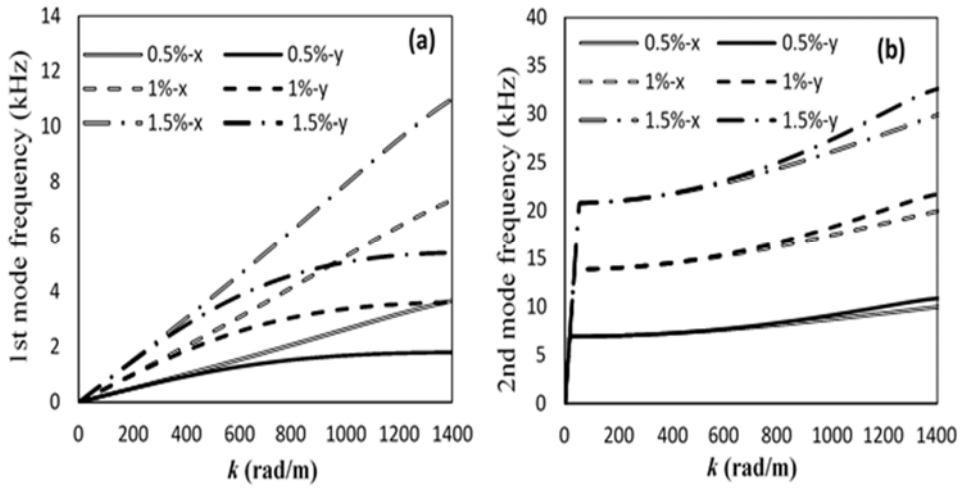

Figure 4.8: Eigenfrequency variation with wave vectors aligned with the material principal directions (i.e., *x* and *y* directions) of the regular honeycomb lattice, showing: a) first mode frequencies and b) second mode frequencies. Results obtained at three relative densities: 0.5%, 1%, and 1.5%.

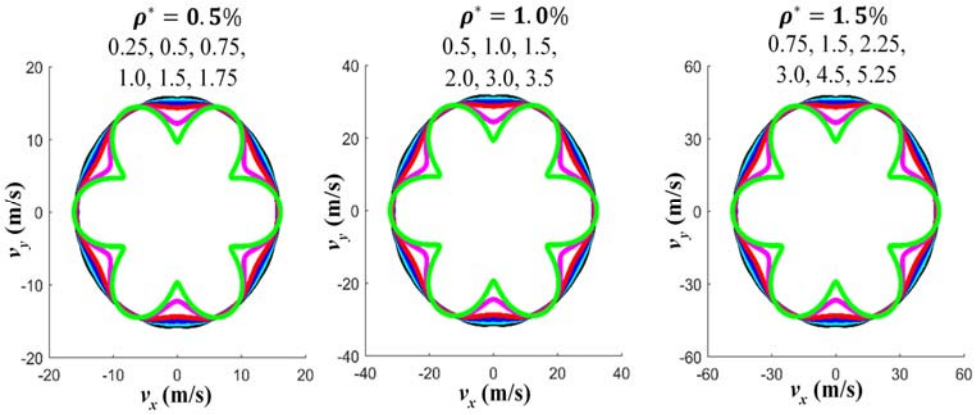

Figure 4.9: Phase velocities corresponding to the 1st Eigenmode of the honeycomb structure. Contour lines in each subplot correspond to the phase velocity vector at the frequencies (kHz) inserted on the top of each subplot. Frequencies from low to high are associated with the contours from the outermost to the innermost.

this figure. Phase velocities along the honeycomb's material principal directions (*x* and *y*) are computed from Figures 4.6 and 4.7 and are plotted against wave vector magnitude in Figure 4.11.

For the first mode, Figure 4.11-a demonstrates a proportional dependence of phase velocity on relative density. It also shows that at larger wave vectors, which

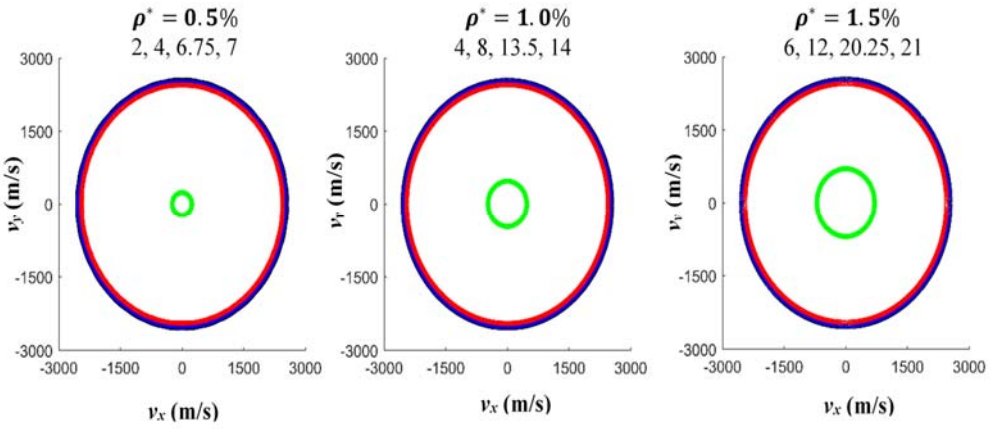

Figure 4.10: Phase velocities corresponding to the 2nd Eigenmode of the honeycomb structure. Contour lines in each subplot correspond to the frequencies (kHz) inserted on the top of each subplot. Frequencies from low to high are associated with the contours from the outermost to the innermost.

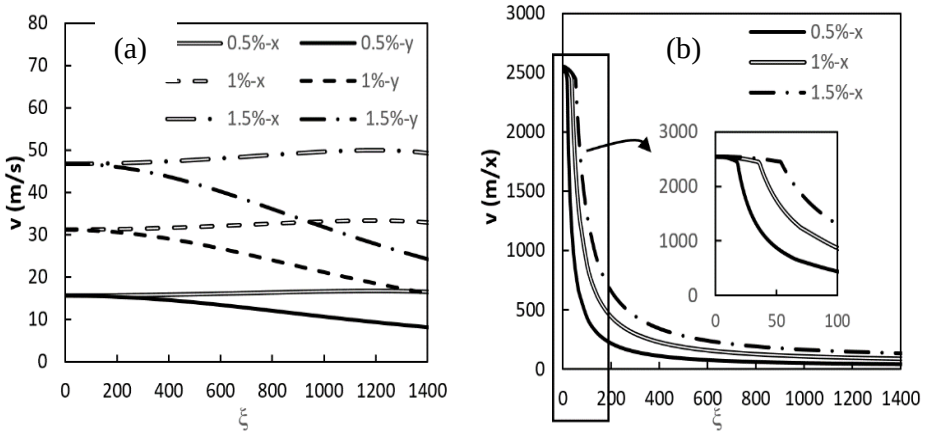

Figure 4.11: Phase velocities along the material principal directions (x, y) of the honeycomb structure, showing phase velocities corresponding to the 1st mode in (a) and the 2nd mode in (b).

translates to larger frequencies, the phase velocity along the *y*-axis drops substantially, while the phase velocity along the *x*-axis exhibits at minor increase. For the second mode, the variation of phase velocity with wave vector along the *x*-direction is practically similar in trends and value to that along the *y*-direction, which is anticipated from Figure 4.8-b. Accordingly, Figure 4.11-b presents the variation along the *x*-direction only. This figure demonstrates an exponentially decaying phase velocity for most of the wave vector range plotted. The observed trend corresponds to the second

and third phases observed phases in Figure 4.8-b. The observed decrease is also linearly dependent on porosity; it scales linearly with relative density. The first phase in Figure 4.8-b, which corresponds to a constant and porosity independent phase velocity, can only be observed when one zooms into the first 100 kHz range of Figure 4.11-b. The insert in Figure 4.11-b presents the zoomed in perspective, and it shows the relatively constant phase velocities (i.e., non-dispersive range) corresponding to the frequency independent initial phase in Figure 4.8-b

4.2.2 Dispersion surfaces and phase velocities of the reinforced honeycomb lattice. For the reinforced honeycomb, constructing the dispersion surfaces requires a slightly modified plotting procedure than for the regular honeycomb case. 1st mode dispersion surfaces of the reinforced honeycomb exhibit steeply increasing frequency contours near the origin of the 1st Brillouin zone (i.e., at very small wave vectors) and slowly decreasing frequency contours at large wave vectors. The latter is indicative of negative group velocities. Creating one plot that clearly and simultaneously demonstrates the different behaviors of the dispersion surfaces is found unfeasible. Multiple figures are needed to demonstrate the different behaviors. For instance, the 1st mode dispersion surfaces of the reinforced honeycomb with 0.5% relative density are shown in Figure 4.12. This figures progressively zooms in the small wave vector region where the contours are clustered. Figure 4.12 demonstrates the existence of two domains: an increasing frequency domain that ends at a frequency of 5 kHz (right plot in Figure 4.12), and a decreasing frequency domain that start at 5 kHz and ends around 3kHz (left plot in Figure 4.12). In this figure, the contours are circular for most of the 1st Brillouin zone, indicating an almost direction independent behavior. This can be attributed to the quasi-isotropic stiffness of the reinforced honeycomb. Unlike the regular honeycomb, which exhibits a load type dependent stiffness (i.e., higher under multiaxial loading than under uniaxial loading) [3], the reinforced honeycomb has to a great extent load and direction independent stiffness [8]. Figure 4.12 also shows contours of decreasing frequency as one moves away from the origin which is indicative of dispersive behavior. Thus, asymmetric waves propagating in the reinforced honeycomb would exhibit in general dispersive but direction independent properties for most of the wave vectors bounded by the 1st Brillouin zone. For the two other relative densities (1% and 1.5%), the 1st mode dispersion surfaces exhibited similar two phase behavior to the one observed in Figure 4.12 for $\rho^* = 0.5\%$. The two other relative

densities just have different transition frequencies between the increasing and decreasing frequency contours. In the following discussion, emphasis is given to the dispersion surfaces with increasing frequencies, which are bounded by the transition frequency. The increasing frequency domain is considered here as it overlaps with the frequencies exhibited by the regular honeycomb, which is used as a benchmark. This facilitates conducting comparison between the responses of the two lattices to satisfy the objective of this work, which emphasizes on demonstrating the effect of the underlying deformation mechanism in lattices (stretching or bending) on their frequency and direction dependent acoustic properties.

For the reinforced honeycomb, 1st mode dispersion surfaces corresponding to the region of the 1st Brillouin zone with increasing frequency contours are shown in Figure 4.13 for the three investigated relative densities. For all cases, Figure 4.13 shows circular contours that expand proportionally. This demonstrates a direction and frequency independent behavior. However, Figure 4.13 shows that the transition frequency, after which the dispersive behavior and the negative nonlinear correlation between frequency and wave vector starts, scales linearly with relative density. The transition frequencies corresponding to the relative densities of 0.5%, 1%, and 1.5% based on Figure 4.6 are 5, 10,15 kHz, respectively. Accordingly, an asymmetric wave propagating in the reinforced honeycomb at a frequency below the transition frequency would exhibit isotropic and non-dispersive behavior.

For the reinforced honeycomb, two phase behavior is also exhibited by its 2nd mode dispersion surfaces. However, 2nd mode frequency contours exhibit an increasing and constant frequency regions separated by a transition frequency. Second mode dispersion surfaces of the reinforced honeycomb, up to the contours corresponding to the transition frequencies, are shown in Figure 4.14. This figure is qualitatively similar to Figure 4.13. Accordingly, symmetric wave propagating in the reinforced honeycomb at a frequency below the transition frequency would exhibit isotropic and non-dispersive behavior. With respect to the effect of relative density, similar to the 1st mode dispersion surfaces, 2nd mode frequency contours and the transition frequencies scale linearly with relative density.

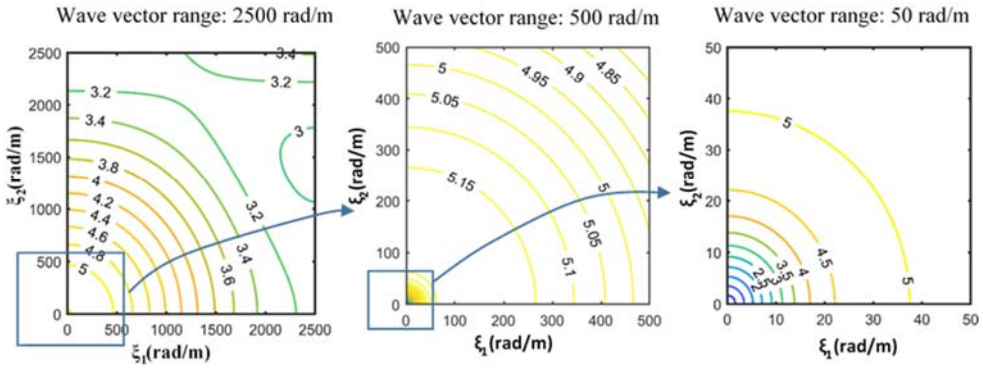

Figure 4.12: Dispersion surfaces corresponding to the 1st Eigenmode of the reinforced honeycomb structure (case 1). Figure progressively show the dispersion surfaces at smaller wave vector values. The middle and right figures are exploded views of the small regions defined by the square inserts in the left and middle figures, respectively.

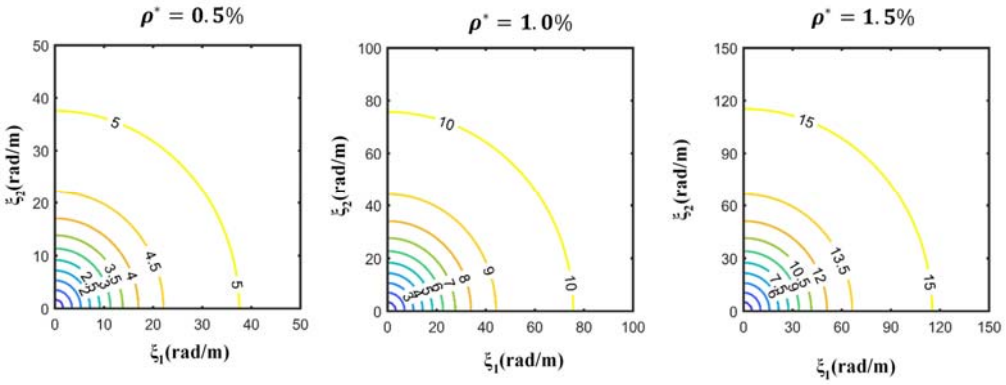

Figure 4.13: Dispersion surfaces corresponding to the 1st Eigenmode of the reinforced honeycomb structure in the range of cell's 1st Brillouin zone exhibiting positive group velocities. Isolines are in kHz and represent the wave vectors, ***k***, corresponding to the same frequency.

The aforementioned discussion of the direction and frequency dependent behavior of the first two eigenmodes was limited mostly to the region of the 1st Brillouin zone with positive correlation between frequency and wave vector. To extend this discussion to cover the whole 1st Brillouin zone, the frequency variation with wave vector is reported along the reinforced honeycomb's material principal directions in Figure 4.15. Subplots a and b in this figure correspond to the 1st mode and 2nd mode, respectively. The behavior along the material principal directions for the reinforced honeycomb suffices to represent the directional and frequency dependent behavior as this lattice is direction independent for most of its 1st Brillouin zone. This is concluded

from the overall behavior shown in Figure 4.12 and since the 2nd mode is less direction dependent than the 1st mode. Figure 4.15 shows the two phase behavior discussed above for the two modes. It demonstrates, for the two modes, similar response along the two material principal directions. It also shows that the frequencies beyond the transition frequency (i.e., in the dispersive region) scale approximately linearly with relative density. For instance, scaling the relative density by 1.5, resulted in scaling the frequencies in the dispersive range by a factor of 1.35~1.5. Here, the 1.35 and 1.5 ratios are observed at the small wave vector range and large wave vector range, respectively.

Using the data of Figure 4.15, the phase velocities, for the first two modes, along the material principal directions of the reinforced honeycomb are computed using $v = \omega/\boldsymbol{k}$**.** As the dispersion surfaces corresponding to the first two modes of the reinforced honeycomb are direction independent for most of the 1st Brillouin range (see the last two paragraphs), it suffices to consider only one direction to characterize the dependence of the reinforced honeycomb's phase velocity on wave vector. Accordingly, the phase velocity of the reinforced honeycomb is represented in Figure 4.16 through its behavior along the *x*-direction. According to Figure 4.16-a, 1st mode phase velocity for all relative densities starts at 1800 m/s and decreases exponentially with increased wave vector magnitude. However, the rate of decrease is higher at lower relative densities and is dependent on the wave vector magnitude. The aforementioned trends apply to the second mode phase velocities shown in Figure 4.16-b. This figure shows that 2nd mode phase velocity, for all relative densities, starts at 3100 m/s and decreases exponentially at larger wave vectors. In addition, the rate of decrease in 2nd mode phase velocity is higher at lower relative densities. It should be noted that Figure 4.16 represents the behavior of the reinforced honeycomb in both non-dispersive and dispersive phases. In the non-dispersive phase, the one demonstrated in Figures 4.13 & 4.14 and is bounded by the transition frequency, phase velocity is independent of frequency, direction, and relative density. This phase corresponds to the linear slope in Figure 4.15 and the start point of Figure 4.16. In this non-dispersive phase, the 1st mode and 2nd mode phase velocities are 1800m/s and 3100m/s, respectively. Since the range of the non-dispersive phase relates to a small region of the 1st Brillouin zone, asymmetric (shear) waves or symmetric (longitudinal) waves propagating in the reinforced honeycomb would exhibit direction independent properties and dispersive properties for most wave vector values.

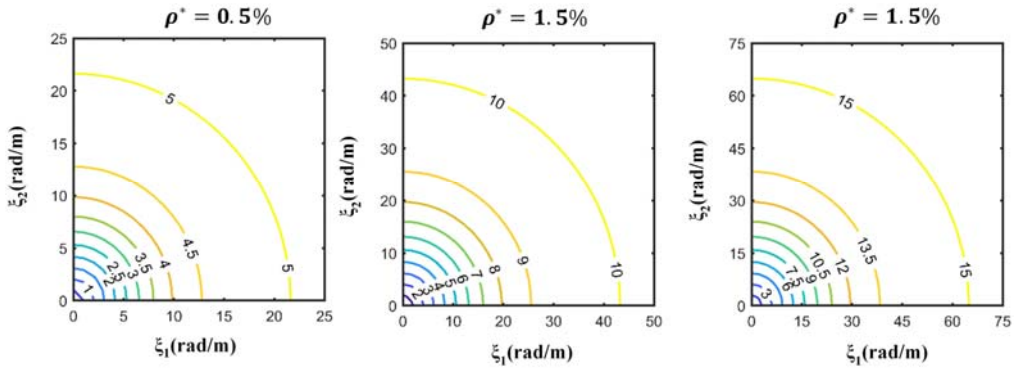

Figure 4.14: Dispersion surfaces corresponding to the 2st Eigenmode of the reinforced honeycomb structure. Isolines are in kHz and represent the wave vectors, ***v***, with the same frequency.

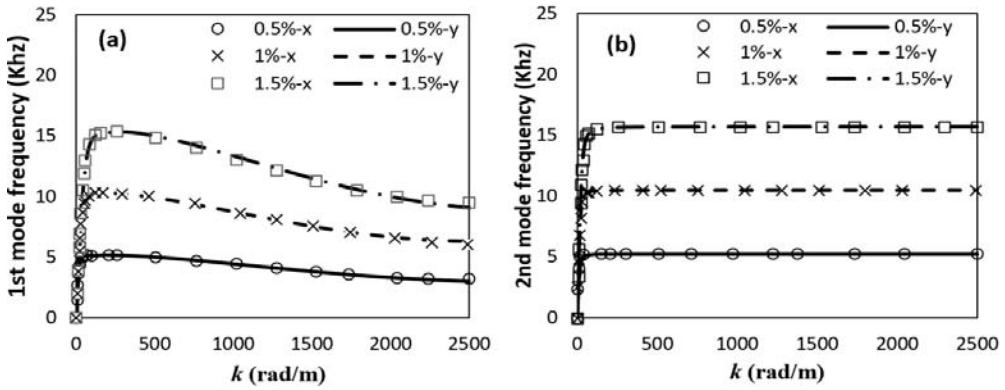

Figure 4.15: Eigenfrequency variation with wave vectors aligned with the material principal directions (i.e., *x* and *y* directions) for the reinforced honeycomb lattice, showing: a) first mode frequencies and b) second mode frequencies. Results obtained at three relative densities: 0.5%, 1%, and 1.5%.

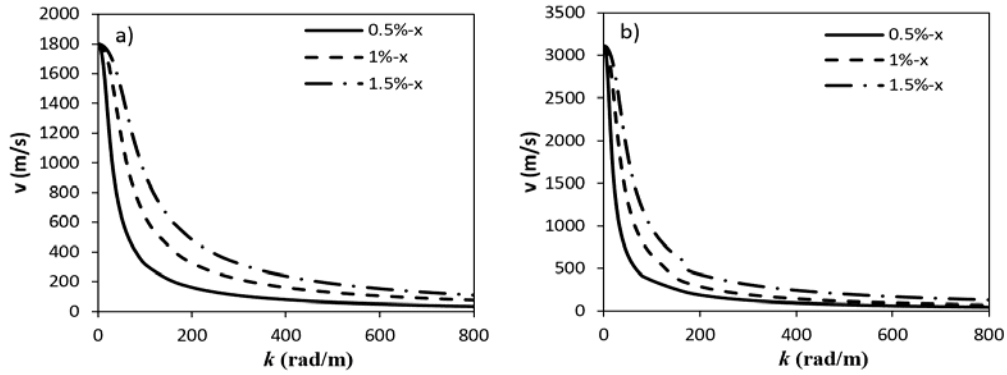

Figure 4.16: Phase velocities along the material principal directions (*x*, *y*) of the reinforced honeycomb, showing phase velocities corresponding to the 1st mode in (a) and the 2nd mode in (b).

Chapter 5. Discussion

First part of this chapter discusses the results describing the acoustic properties of double sided honeycombs included in the preceding chapter. Subsequently, a comparison is conducted between the results obtained from the bending dominated and stretching dominated lattices analyzed in the results chapter.

5.1 Effect of Double-sided Walls in Hexagonal Honeycomb

Low sub-ultrasound frequencies have been proven useful in the nondestructive evaluation of periodic honeycomb aluminum structures [4]. However, to use them in the inspection of double-sided honeycombs, it is instrumental to have a detailed priori knowledge of the low frequency wave propagation characteristics in the inspected honeycomb. This knowledge is essential for properly selecting the frequency that matches the inspected medium; positioning the sensors, wave sources and receivers; and for interpreting the collected data. Figures 4.4 and 4.5 readily provide in a graphical manner the most relevant characteristics pertaining to the low wave propagation characteristics in the double-sided honeycombs analyzed in this work, which are widely used in composite sandwiched structures. Not only they show the wave phase velocity in terms of propagation direction, frequency and deformation mode, but they also show the frequencies at which the honeycombs are isotropic and nondispersive. These frequencies would be most suited to be employed in the nondestructive testing of aluminum honeycombs. Inasmuch, these results have some important features that are discussed in this section, mainly to better understand the behavior seen in Figures 4.4 and 4.5.

In general, asymmetric (Figure 4.4) and symmetric (Figure 4.5) waves exhibit different characteristics as the underlying deformation mechanisms associated with each of them are different. Figure 4.1 presents clear differences between the deformation patterns corresponding to the asymmetric and symmetric deformation modes. Deformations corresponding to the asymmetric mode are localized in few cell walls and most of the deformation is achieved by twisting (rotation) of vertices (i.e., the intersections between three cell walls). On the contrary, most cell walls undergo significant deformations in the symmetric deformation mode.

In the nondispersive frequencies range, asymmetric waves exhibit equal phase velocities along the material principal directions. This behavior mirrors the expected elastic response of the double-sided honeycombs under static loads, which are proven to have equal elastic moduli along their two material principal directions [3]. This behavior is attributed to the fact that the nondispersive frequencies are small and have wave lengths that significantly exceed the cell size of the honeycombs. For example, case 1 exhibited equal phase velocities along the x- and y- directions at 3 kHz. The wave vector corresponding to the 3 kHz contour line (inner most contour line for case 1 in Figure 4.2) is ~250 rad/m. This results in a wave length of ~25 mm, which is roughly 15 times larger than the cell size of case 1. Accordingly, at the 3 kHz frequency, case 1 is anticipated to exhibit a response reminiscent of its properties under static loading, which is quasi-isotropic with equal elastic moduli along the material principal direction [3]. The aforementioned analysis, which used case 1 as an example, applies to all case, though the frequency level at which it applies can be different and depends on the cell size.

The observed equality in phase velocities along the two material principal directions in its nondispersive frequency range was also verified using direct explicit simulations. These simulations were performed on full models made by reproducing the unit cell of Figure 3.3 to create a multi-cell structure. Full-scale models were subjected to asymmetric wave generating boundary conditions. For illustration, the finite element models for case 1 along with the resulting deformations due to asymmetric waves are shown in Figure 5.1. To measure the phase velocity along the x-axis, a sinusoidal displacement boundary condition, $= 1 \times 10^{-3} \sin(2\pi f t)$ mm , with a frequency of 3 kHz was applied on the left side of the structure to generate a horizontally propagating (left to right) asymmetric wave. Phase velocity was then computed as the ratio of the cell size to the time required for the wave to pass through a full cell near the middle of the specimen. A cell in the middle was chosen to be far away from the boundary where load was applied and far away from the perimeter to avoid the interference caused by reflected waves. Computed phase velocity was 93.3 m/s which agrees with the one reported in Figure 4.4. Similarly, to determine the phase velocity along the y-direction, the aforementioned process was repeated, but a sinusoidal displacement boundary condition, $u = 1 \times 10^{-3} \sin(2\pi f t)$ mm, with a frequency of 3 kHz was imposed on the top side of the structure to generate a downward

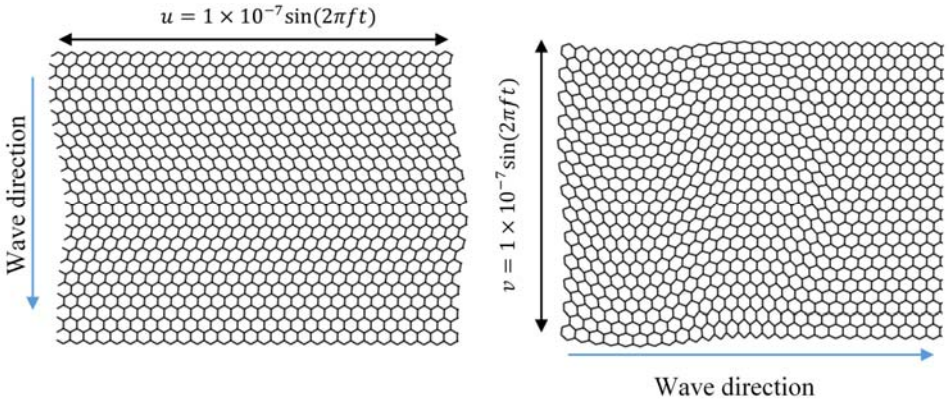

Figure 5.1: Asymmetric wave propagation in a multi-cell honeycomb made by periodically repeating the unit cell from case 1. Showing a vertically propagating wave (left) and a horizontally propagating wave (right). Frequency (f) is 3 kHz and deformation is scaled by 10^5 to enhance visibility.

moving asymmetric wave. Phase velocity in the y-direction was computed as 92.8 m/s which is relatively equal to the horizontal phase velocity, confirming the equivalence in phase velocities along the honeycomb material principal directions.

Phase velocities in the nondispersive frequency range are dependent on relative density; a clear positive correlation can be seen in Figure 4.4. The correlation is found by plotting the velocities along the material principal directions against relative density to be linear. The linear dependence can be explained analytically using Eqn. (8) in conjunction with the following classical scaling laws developed for predicting the relative density and elastic moduli of double sided honeycombs [3]

$$\frac{G_{xy}}{E_{solid}} = 0.102\left(\frac{t}{l}\right)^3, \frac{E_x}{E_{solid}} = \frac{E_y}{E_{solid}} = 2.31\left(\frac{t}{l}\right)^3, \frac{\rho}{\rho_{solid}} = 2.87\left(\frac{t}{l}\right) \qquad (12)$$

based on this equation, the longitudinal and shear moduli of double sided honeycombs have a third order dependence on relative density (i.e., ~$[\rho/\rho_{solid}]^3$). Thus, the stiffness matrix, $[\bar{\boldsymbol{K}}]$, which is linearly dependent on honeycombs' moduli, has a third order dependence on relative density. On the other hand, the mass matrix, $[\bar{\boldsymbol{M}}]$, in Eqn. (8) is linearly dependent on relative density. Accordingly, and based on Eqn. (8), the angular frequency (ω) is predicted to have a linear dependence on relative density.

Symmetric waves in the nondispersive frequency range are independent of relative density. This is highlighted by the similarity of the outermost contours for all the cases in Figure 4.4. Such behavior is convenient for nondestructive inspection as

one would expect the same phase velocity regardless of the honeycomb relative density. This behavior, though unintuitive, can be explained using micromechanical models used to predict the moduli of double-sided honeycombs under multiaxial loading [3] in conjunction with the deformation patterns illustrated in Figure 4.1. Micromechanical models illustrate that the moduli of double-sided honeycombs under multiaxial compressive loads depend linearly on relative density. On the other hand, symmetric deformation patterns shown in Figure 4.1 are very different from their asymmetric counterparts and demonstrate multiaxial deformation patterns, compatible with deformations due to multiaxial compressive loading [3]. Thus, moduli for symmetrically deforming honeycombs depend linearly on relative density. Accordingly, both stiffness $[\bar{\boldsymbol{K}}]$ and mass matrices $[\bar{\boldsymbol{M}}]$ for the cases with symmetric deformations are linearly dependent on relative density. As both $[\bar{\boldsymbol{K}}]$ and $[\bar{\boldsymbol{M}}]$ scale linearly with relative density, the angular frequency, which is a function of their ratio, is independent of relative density.

5.2 Comparison Between Bending-dominated and Stretching-dominated Lattices

The two lattices analyzed are geometrically related and belong to the family of lattices whose building block utilizes hexagonal topology. The reinforced honeycomb lattice is derived from the regular honeycomb lattice and shares with it many topological features. The two lattices have identical relative densities and planes of symmetry. The main difference between the two lattices is their main admissible deformation mode. Whereas the hexagonal lattice deforms mostly through the bending of its ligaments, the reinforced lattice deforms mainly through the stretching of its ligaments. Bending deformation in the reinforced lattice is negligible. The difference in the dominant deformation mode between the two lattices result in significant differences in their acoustic properties. The full analysis of the behavior of the two lattices due to asymmetric and symmetric propagating waves is detailed in the previous two section. However, based on it, major differences can be highlighted.

Asymmetric propagating waves are more direction dependent in the regular honeycomb than in the reinforced honeycomb. The regular honeycomb is direction independent at low frequencies and dependent at high frequencies. However, the reinforced honeycomb is direction independent for most frequencies. On the other hand, asymmetric propagating waves are more dispersive in the reinforced honeycomb than

in the regular honeycomb. The regular honeycomb can be non-dispersive at a wide range of wave vectors; however, the reinforced honeycomb is non-dispersive in a very small range of wave vectors. In addition, asymmetric waves have lower phase velocities in the regular honeycomb than in the reinforced honeycomb, lower by two orders of magnitude at small wave vector magnitudes. Finally, phase velocity of asymmetric waves scale linearly with relative density in the regular honeycomb, but it scales nonlinearly with relative density in the reinforced honeycomb.

Symmetric waves are relatively direction independent and mostly dispersive for both regular and reinforced honeycombs. For both lattices, the non-dispersive behavior is associated with a very small wave vector range. Phase velocity of symmetric waves is higher in the reinforced honeycomb by ~24%. For both lattices, phase velocity decrease significantly with increased wave vector magnitude. The rate of decrease increases with decreasing relative density. Finally, phase velocity of symmetric wave scales approximately linearly with relative density in regular honeycombs (in the dispersive phase), but nonlinearly with relative density in the reinforced honeycomb (also in the dispersive phase). Phase velocity of symmetric waves is direction, frequency, and relative density independent in the non-dispersive phase.

Chapter 6. Conclusions

This work uses finite element analysis as a criterion for understanding the underlying physics of elastic wave propagation at low to sub-ultrasound frequencies in aluminum honeycombs made by bonding thin corrugates sheets. Selected honeycomb structures for this study are representative of commercial aluminum honeycombs used as cores in composite sandwiched structures. A wide range of relative densities, sheet thicknesses, and cell sizes are considered to represent the various commercially available hexagonal aluminum honeycombs.

Properties of shear and longitudinal elastic waves in terms of phase velocity, dispersion, and dependence on propagation direction are determined for a wide range of frequencies, ranging from infrasound to ~10^2 kHz. Obtained results provide the phase velocity and dispersion properties of shear and longitudinal waves for every in-plane propagation direction and for a wide range of relative densities and cell sizes. These results are instrumental for nondestructive inspection methodologies tailored for using low and sub-ultrasound frequencies to inspect honeycombs made from corrugated sheets.

Moreover, results show that shear and longitudinal waves exhibit nondispersive behavior at low frequencies, lower than a frequency limit. This limit increases with the increase in relative density or sheet thickness as well as with the decrease in cell size. In the nondispersive frequency range, phase velocity for shear waves are direction dependent and linearly dependent on relative density. However, shear phase velocities along the material principal directions are identical. On the other hand, in the nondispersive frequencies range, phase velocity for longitudinal waves are independent of direction and relative density. In general, results illustrate that the dispersive and direction dependent behavior is more significant at higher frequencies and higher porosities. In addition, the frequencies at which nondispersive behavior commences are higher for honeycombs with higher densities.

Results represent a map that can be used to determine the speed of sound for in-plane waves in honeycombs made from corrugated sheets. Moreover, trends highlighted and discussed, which relate phase velocity to relative density, allow for generalizing the results obtained in this work through simple scaling to honeycombs made from corrugated sheets of any metal.

The direction and frequency dependent acoustic behavior of a topologically related bending dominated (i.e., regular honeycomb) and stretching dominated (i.e., reinforced honeycomb) lattices was analyzed using computational methods in this work. The objective was to highlight the differences in the acoustic response of the two lattice architectures due to the difference in their deformation mechanisms. Results and discussion support the following conclusions.

- Although the two considered lattices have identical relative densities, cell sizes, and planes of symmetry, elastic waves propagating through them exhibited different behaviors, in terms of waves' direction dependence and phase velocities. These differences are attributed to the lattices' dissimilar deformation modes at their ligaments level.
- Symmetric waves exhibited mostly direction independent behavior in the stretching dominated lattice. On the other hand, in the bending dominated lattice, they exhibited mild direction dependence at wave lengths smaller than 4.5 times the lattice's cell size and direction independent behavior at larger wave lengths.
- Asymmetric waves exhibited mostly direction independent behavior in the stretching dominated lattice. However, in the bending dominated lattice, they exhibited significant direction dependent behavior at wave lengths smaller than 8.4 times the lattice's cell size and direction independent behavior at larger wave lengths.
- The relation between phase velocity of asymmetric waves and relative density is linear in the bending the dominated lattice and nonlinear in the stretching dominated lattice.
- The relation between phase velocity of symmetric waves and relative density, in the dispersive range, is approximately linear for the bending dominated lattice and nonlinear for the stretching dominated lattice.
- Phase velocities are higher in the stretching dominated lattice than in the bending dominated lattice. Higher by up to two orders of magnitude in the asymmetric waves case, and up to ~25% in the symmetric waves case.
- Both lattices exhibited dispersive behavior that increased with decreasing their relative density, for both asymmetric and symmetric waves.

Results of the present work demonstrate the potential for realizing lattice architectures with tailored acoustic behavior. For instance, by transforming a lattice between the two states of being bending dominated or stretching dominated, one can increase or decrease its phase velocities and stiffness without affecting its weight or size.

References

[1] A. K. Kaw, *Mechanics of composite materials*: CRC press, 2005.

[2] I. M. Daniel, O. Ishai, I. M. Daniel, and I. Daniel, *Engineering mechanics of composite materials*, sheffield, UK: Oxford university press New York, 1994.

[3] L. Gibson, J. and M. Ashby, F., *Cellular Solids: Structure and Properties*, Cambridge, UK: Cambridge University Press, 1997.

[4] S. Thwaites and N. Clark, "Non-destructive testing of honeycomb sandwich structures using elastic waves," *Journal of sound and vibration*, vol. 187, pp. 253-269, 1995.

[5] M. Collet, M. Ouisse, M. Ruzzene, and M. N. Ichchou, "Floquet–Bloch decomposition for the computation of dispersion of two-dimensional periodic, damped mechanical systems," *International Journal of Solids and Structures*, vol. 48, pp. 2837-2848, 10/1/ 2011.

[6] L. Brillouin, *Wave propagation in periodic structures: electric filters and crystal lattices*, New York, USA: DoverPublications, 2003.

[7] M. F. Ashby, T. Evans, N. Fleck, J. W. Hutchinson, and H. N. G. Wadley, *Metal Foams: A Design Guide*: Butter Worth-Heinemann, 2000.

[8] M. Alkhader and M. Vural, "Mechanical response of cellular solids: Role of cellular topology and microstructural irregularity," *International Journal of Engineering Science*, vol. 46, pp. 1035-1051, 2008.

[9] M. Alkhader and M. Vural, "The partition of elastic strain energy in solid foams and lattice structures," *Acta Materialia*, vol. 57, pp. 2429-2439, 2009.

[10] M. Alkhader and M. Vural, "An energy-based anisotropic yield criterion for cellular solids and validation by biaxial FE simulations," *Journal of the Mechanics and Physics of Solids*, vol. 57, pp. 871-890, 2009.

[11] M. Alkhader and M. Vural, "A plasticity model for pressure-dependent anisotropic cellular solids," *International Journal of Plasticity*, vol. 26, pp. 1591-1605, 2010.

[12] N. A. Tamimi, M. Alkhader, B. Ali, and M. Nazzal, "Effect of hierarchical features on the critical buckling strength of periodic cellular solids," in *2020 Advances in Science and Engineering Technology International Conferences, Dubai, UAE*, 2020, pp. 1-5.

[13] H. E. Mir, M. Alkhader, P. D. Pour, and M. Mustafa, "Improving the buckling strength of honeycomb cores using periodic imperfections," in *2020 Advances in Science and Engineering Technology International Conferences, Dubai, UAE*, 2020, pp. 1-6.

[14] M. Alkhader, S. Iyer, W. Shi, and T. Venkatesh, "Low frequency acoustic characteristics of periodic honeycomb cellular cores: The effect of relative density and strain fields," *Composite Structures*, vol. 133, pp. 77-84, 2015.

[15] M. Ruzzene and F. Scarpa, "Directional and band-gap behavior of periodic auxetic lattices," *physica status solidi (b)*, vol. 242, pp. 665-680, 2005.

[16] A. Spadoni, M. Ruzzene, S. Gonella, and F. Scarpa, "Phononic properties of hexagonal chiral lattices," *Wave Motion*, vol. 46, pp. 435-450, 2009.

[17] M. Alkhader, B. Abu-Nabah, M. Elyoussef, and T. A. Venkatesh, "Design of honeycomb structures with tunable acoustic properties," *MRS Advances*, vol. 4, pp. 2409-2418, 2019.

[18] S. Iyer, "Electromechanical Response of Piezoelectric Cellular Architectures: The effect of topological features and deformation modes," Doctor of Philosophy, State University of New York at Stony Brook, USA, 2014.
[19] M. Ruzzene, F. Scarpa, and F. Soranna, "Wave beaming effects in two-dimensional cellular structures," *Smart materials and structures*, vol. 12, p. 363, 2003.
[20] S. Iyer, M. Alkhader, and T. Venkatesh, "Band Gaps in Bravais Lattices Inspired Periodic Cellular Materials and the Effect of Relative Density and Strain Fields," in *ASME 2014 International Mechanical Engineering Congress and Exposition*, 2014, pp. V013T16A022-V013T16A022.
[21] S. Iyer, M. Alkhader, and T. A. Venkatesh, "Electromechanical Response of Piezoelectric Honeycomb Foam Structures," *Journal of the American Ceramic Society*, vol. 97, pp. 826-834, 2013.
[22] S. Iyer, M. Alkhader, and T. Venkatesh, "Electromechanical behavior of auxetic piezoelectric cellular solids," *Scripta Materialia*, vol. 99, pp. 65-68, 2015.
[23] W. Liu, L. Lv, Y. Li, Y. Wang, J. Wang, C. Xue, *et al.*, "Effects of slurry composition on the properties of 3-1 type porous PZT ceramics prepared by ionotropic gelation," *Ceramics International*, vol. 34, pp. 6542-6547 2017.
[24] M. H. Yousuf, W. Abuzaid, and M. Alkhader, "4D printed auxetic structures with tunable mechanical properties," *Additive Manufacturing*, vol. 35, p. 101364, 2020/10/01/ 2020.
[25] W. Abuzaid, M. Alkhader, and M. Omari, "Experimental analysis of heterogeneous shape recovery in 4d printed honeycomb structures," *Polymer Testing*, vol. 68, pp. 100-109, 2018/07/01/ 2018.
[26] K. Bertoldi and M. Boyce, "Mechanically triggered transformations of phononic band gaps in periodic elastomeric structures," *Physical Review B*, vol. 77, p. 052105, 2008.
[27] H. Cui, R. Hensleigh, D. Yao, D. Maurya, P. Kumar, M. G. Kang, *et al.*, "Three-dimensional printing of piezoelectric materials with designed anisotropy and directional response," *Nature materials*, vol. 18, pp. 234-241, 2019.
[28] S. Iyer, M. Alkhader, and T. A. Venkatesh, "On the relationships between cellular structure, deformation modes and electromechanical properties of piezoelectric cellular solids," *International Journal of Solids and Structures*, vol. 80, pp. 73-83, 2016/02/01/ 2016.
[29] Y. He, S. Guo, Z. Liu, and K. Liew, "Pattern transformation of thermo-responsive shape memory polymer periodic cellular structures," *International Journal of Solids and Structures*, vol. 71, pp. 194-205, 2015.
[30] M. Di Prima, K. Gall, D. McDowell, R. Guldberg, A. Lin, T. Sanderson, *et al.*, "Deformation of epoxy shape memory polymer foam. Part I: Experiments and macroscale constitutive modeling," *Mechanics of Materials*, vol. 42, pp. 304-314, 2010.
[31] M. Alkhader, W. Abuzaid, M. Elyoussef, and S. Al-Adaileh, "Localized strain fields in honeycomb materials with convex and concaved cells," *European Journal of Mechanics - A/Solids*, vol. 80, p. 103890, 2020/03/01/ 2020.
[32] M. Alkhader and M. Vural, "Influence of Cellular Topology on Dynamic Response of Solid Foams," in *ASME 2006 International Mechanical Engineering Congress and Exposition, Chicago, Illinois, USA*, 2006, pp. 199-206.

[33] A. Ahmed, M. Alkhader, and B. Abu-Nabah, "In-plane elastic wave propagation in aluminum honeycomb cores fabricated by bonding corrugated sheets," *Journal of Sandwich Structures & Materials,*vol. 21, pp. 1-26, 2017.

[34] V. S. Deshpande, M. F. Ashby, and N. A. Fleck, "Foam topology: bending versus stretching dominated architectures," *Acta Materialia,* vol. 49, pp. 1035-1040, 4/2/ 2001.

[35] M. Alkhader, M. Nazzal, and K. Louca, "Design of bending dominated lattice architectures with improved stiffness using hierarchy," *Proceedings of the Institution of Mechanical Engineers Part C-Journal of Mechanical Engineering Science,* vol. 233, pp. 3976-3993, Jun 2019.

[36] M. Alkhader and M. Vural, "Effect of Microstructure in Cellular Solids: Bending vs. Stretch Dominated Topologies," in *Recent Advances in Space Technologies, 2007. RAST '07. 3rd International Conference, Istanbul, Turkey*, 2007, pp. 136-143.

[37] A. S. Phani, J. Woodhouse, and N. Fleck, "Wave propagation in two-dimensional periodic lattices," *The Journal of the Acoustical Society of America,* vol. 119, pp. 1995-2005, 2006.

[38] S. Gonella and M. Ruzzene, "Analysis of in-plane wave propagation in hexagonal and re-entrant lattices," *Journal of Sound and Vibration,* vol. 312, pp. 125-139, 2008.

[39] S. Mukherjee, F. Scarpa, and S. Gopalakrishnan, "Phononic band gap design in honeycomb lattice with combinations of auxetic and conventional core," *Smart Materials and Structures,* vol. 25, p. 054011, 2016.

[40] Y. Liu, X.-z. Sun, and S.-t. Chen, "Band gap structures in two-dimensional super porous phononic crystals," *Ultrasonics,* vol. 53, pp. 518-524, 2013.

Vita

Ammar Ahmed was born in 1993, in Dundee, UK. He received his primary and secondary education in Khartoum, Sudan. He received his B.Sc. degree in Mechanical Engineering from the Khartoum University, Sudan in 2015.

In September 2016, he joined the Mechanical Engineering master's program in the American University of Sharjah as a graduate teaching assistant. His research interests are in finite element simulations, computer aided design and Non-destructive testing.